BIOPHYSICS

Self-assembly–based posttranslational protein oscillators

Ofer Kimchi[1]*, Carl P. Goodrich[1], Alexis Courbet[2,3,4], Agnese I. Curatolo[1], Nicholas B. Woodall[2,3,4], David Baker[2,3,4], Michael P. Brenner[1,5]

Recent advances in synthetic posttranslational protein circuits are substantially impacting the landscape of cellular engineering and offer several advantages compared to traditional gene circuits. However, engineering dynamic phenomena such as oscillations in protein-level circuits remains an outstanding challenge. Few examples of biological posttranslational oscillators are known, necessitating theoretical progress to determine realizable oscillators. We construct mathematical models for two posttranslational oscillators, using few components that interact only through reversible binding and phosphorylation/dephosphorylation reactions. Our designed oscillators rely on the self-assembly of two protein species into multimeric functional enzymes that respectively inhibit and enhance this self-assembly. We limit our analysis to within experimental constraints, finding (i) significant portions of the restricted parameter space yielding oscillations and (ii) that oscillation periods can be tuned by several orders of magnitude using recent advances in computational protein design. Our work paves the way for the rational design and realization of protein-based dynamic systems.

INTRODUCTION

Protein oscillators play a major regulatory role in organisms ranging from prokaryotes to humans. In most known biological cases, the oscillation is realized through transcription/translation cycles. Few examples of purely posttranslational oscillators have been found in biology (*1*, *2*). At the same time, posttranslational protein circuits are increasingly sought after for synthetic applications, since they have the potential to exhibit faster response to environment changes, allow for more direct control over the circuit behavior, be directly coupled to a functional output, and can be used in contexts that do not include the vast genetic apparatus (*3*–*5*). While significant recent work has enabled the design of synthetic posttranslational protein–based logic gates (*4*, *5*), engineering tunable dynamic phenomena such as oscillations in a synthetic posttranslational context remains an outstanding challenge (*6*, *7*).

The best-studied example of biological posttranslational protein oscillators is the KaiABC system in cyanobacteria (*8*). By placing only the proteins KaiA, KaiB, and KaiC in a test tube, along with abundant adenosine triphosphate, the KaiC proteins collectively get sequentially phosphorylated and dephosphorylated, forming an oscillatory cycle (*9*, *10*). While the KaiC proteins generally exist in a hexameric state, monomers are shuffled among the hexamers during only a certain phase of the oscillatory cycle (*11*). The KaiABC system demonstrates that protein oscillators need not use transcription/translation cycles or large numbers of components to achieve oscillatory behavior.

Motivated by the KaiABC system, we set out to design a protein-based oscillator that could be reconstituted in vitro using only a small number of components at relatively high copy numbers, so that any resulting oscillations are not stochastic. To facilitate the future translation of this theoretical study to an experimental system, we base the architecture of our system on biochemical constraints and on a design space navigable through computational protein design. We constrain the kinetic reaction network to only include three protein species and to only allow reversible binding and phosphorylation/dephosphorylation enzyme reactions.

As in KaiABC, the oscillating system will cycle through periods of a protein species being phosphorylated or not. When the target protein is phosphorylated, the phosphorylation must induce a change to propel the global state along the oscillatory cycle. This change can be achieved by affecting the enzyme kinetics of the kinase and phosphatase in one of two ways: either by altering the conformation of the target protein or by directly modifying the kinase and phosphatase enzymes. We first consider systems that do not modify the kinase or phosphatase.

The simplest such system, a protein with one phosphorylation site being modified by a kinase and a phosphatase, cannot yield oscillations regardless of parameter choices (*7*). When two phosphorylation sites are included, oscillations are possible only under the assumption that each of the four possible phosphorylation states has significantly different rates of subsequent phosphorylations and dephosphorylations (*7*). While biology seems to have designed a system in KaiABC capable of undergoing the many conformational changes necessary to implement this form of oscillations (*9*), the design of even two (let alone several) protein structures from the same sequence remains a significant challenge for the field of computational protein design (*12*).

These challenges are not unique to molecules with two phosphorylation sites. For example, since oscillations for molecules with two phosphorylation sites are effected by enzyme sequestration (*7*), we consider a molecule containing a single phosphorylation site alongside a kinase- or phosphatase-sequestering domain (or a binding domain for an external compound that itself contains an enzyme-binding domain). These systems are capable of producing oscillations—but only if phosphorylation and binding accompany a significant conformational change in the molecule that modifies the rate constants of subsequent reactions. Even assuming that such a conformational

[1]Harvard University School of Engineering and Applied Sciences, Cambridge, MA 02138, USA. [2]Department of Biochemistry, University of Washington, Seattle, WA 98105, USA. [3]Institute for Protein Design, University of Washington, Seattle, WA 98105, USA. [4]Howard Hughes Medical Institute, University of Washington, Seattle, WA 98105, USA. [5]Kavli Institute for Bionano Science and Technology Harvard University, Cambridge, MA 02138, USA.
*Corresponding author. Email: okimchi@g.harvard.edu

change were designed, we have found no evidence of sustained oscillations in these systems within the parameter regimes of typical binding/unbinding rate constants and typical kinase and phosphatase activity (i.e., the catalytic rate and Michaelis constants k_{cat} and K_M, discussed further below). See section S1 for further discussion.

Systems that focus on modifications to the enzymes themselves are therefore more likely candidates for the production of experimentally realizable oscillations. Biology has found several ways to tie phosphorylation to enzymatic activity. The most straightforward conceptually, having the activity of an enzyme dependent on its own phosphorylation state (*13*) remains a challenge to implement in the context of computational protein design (*14*). However, the field has achieved remarkable success in the design of protein-protein interactions (*15*) which can be modified by phosphorylation (*16*, *17*).

Bootstrapping off of this success, we consider proteins that self-assemble into multimeric functional kinases and phosphatases (*18*, *19*). We are motivated, in part, by the success of using split proteases to implement posttranslational protein–based logic gates (*4*, *5*). In our design, when the proteins' binding interfaces are phosphorylated, their self-assembly is impeded, reducing the concentration of functional enzymes available in the system.

Oscillations are thus achieved by the push and pull of two opposing factors: Self-assembled kinases inhibit the self-assembly of new proteins by phosphorylating both kinase and phosphatase monomers; meanwhile, self-assembled phosphatases counteract this inhibition. Incoherent inputs such as these are known to enhance the robustness of oscillations (*20*). Our overall oscillator design is motivated by analogy to known successful oscillators, particularly the dual-feedback genetic oscillator (*1*, *21*–*23*). Just as that oscillator relies on the interplay between the inhibiting effects of LacI and the activating effects of AraC, our oscillations rely on the interplay between kinase and phosphatase multimers, which respectively inhibit and activate their own self-assembly (Fig. 1A).

The rest of our manuscript is organized as follows. First, we describe the oscillatory circuits and their experimental constraints. Next, we develop simplified mathematical models for two distinct protein-based oscillators: In one, multimers are designed to form closed, bounded structures; in the other, they form unbounded fibers. We show that simple analytical formulae describing the first oscillator can predict both the regions of parameter space admitting oscillations and the oscillations' resulting frequencies. We then demonstrate that the second oscillator design is complementary to the first in that it can admit robust and experimentally realizable oscillations in a regime of parameter space where the first cannot. Finally, we discuss the significance of our findings.

RESULTS

Self-assembly–based protein oscillators are designed within experimental constraints

Designed synthetic oscillators rely on few protein species with specified interactions

The main components of our oscillators are two proteins, which we call κ and ρ. Each individual protein of type κ (ρ) has two complementary parts of a split kinase (phosphatase) and a phosphorylation site. When the respective sites are dephosphorylated, copies of protein κ (ρ) can self-assemble into a functional kinase (phosphatase), which we call K (P). Thus, self-assembled kinases inhibit the self-assembly of new proteins, while self-assembled phosphatases counteract the inhibition. In addition to the proteins κ and ρ, we include a constitutive phosphatase $\tilde{P}$; without it, a fixed point where all proteins are phosphorylated can preclude oscillations (see section S2).

The resulting circuit topology (Fig. 1A) is analogous to that used in the dual-feedback genetic oscillator (*1*, *23*). The multimeric kinase plays an analogous role to the LacI protein in the genetic oscillator, repressing the production of new multimers; the multimeric phosphatase plays an analogous role to that of the AraC protein, activating the production (or more precisely, counteracting the kinase inhibition).

Two related networks based on these proteins can be designed. In the first, self-assembly is into closed symmetric homomultimers of specified size; in the second, the monomers are designed such that they self-assemble into one-dimensional unbounded fibers.

Experimental realizability constrains parameter sets

Because we are motivated by experimental feasibility, we consider only physically realizable parameters for our models. Binding rates

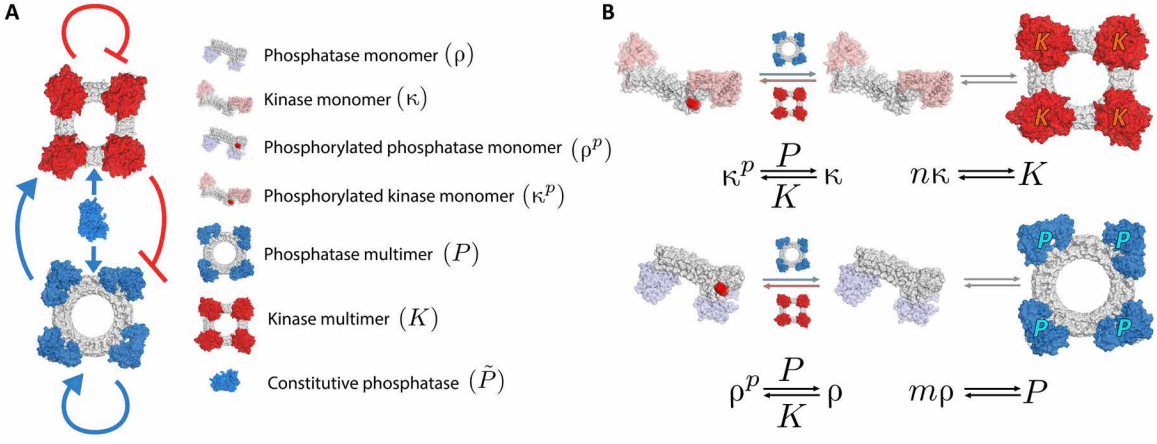

Fig. 1. Bounded self-assembly oscillator. (**A**) Oscillator topology. By phophorylating monomers, kinase multimers (red; top) inhibit their own and phosphatase multimer (blue; bottom) self-assembly. Similarly, phophatase multimers counteract this inhibition, as do constitutive phosphatases (center). (**B**) Bounded self-assembly reactions. Monomers contain two halves of a split enzyme: either kinase (red; top) or phosphatase (blue; bottom). Monomers can self-assemble into multimers of specified size (here, tetramers are pictured, corresponding to $n = m = 4$). Kinase (phosphatase) multimers can (de)phosphorylate the monomers. A constitutive phosphatase is also able to dephosphorylate the monomers (not pictured). Phosphorylated monomers cannot participate in the self-assembly. Reactions are shown in pictorial form above each corresponding chemical equation. The full set of differential equations corresponding to these reactions is given in eq. S1.

k_b are typically in the range 10^{-2} to 10^{0} $\mu M^{-1}s^{-1}$ (*24*) with dissociation constants k_d typically in the 10^{-3} to 10^{3} μM range (*25*). Both of these quantities can be tuned on the basis of the geometry, energy, and symmetry of the binding interface between the proteins, which we assume here to be designed de novo. Less straightforward to design are the Michaelis constants and catalytic rates of the kinase and phosphatase, especially since these depend not only on the enzyme but on the substrate. Mutational screens can be used to adjust these parameters, but predicting the effect of a mutation on k_{cat} or K_M is highly nontrivial (*26*). We were unable to find studies measuring kinase and phosphatase rates on the same substrate. Instead, as a standard to demonstrate physical realizability, we consider the parameters for sample Ser/Thr enzymes: wild-type λ-phosphatase acting on para-nitrophenylphosphate ($k_{cat} = 2.0 \times 10^{3}$ s^{-1}; $K_M = 1.0 \times 10^{4}$ μM) and wild-type MST4 (kinase) acting on the short peptide chain NKGYNTLRRKK ($k_{cat} = 3.1$ s^{-1}; $K_M = 14$ μM) (*26*, *27*). We assume throughout that the constitutive phosphatase $\widetilde{P}$ is governed by the same enzymatic rate constants as the self-assembled *P*. We also treat the self-assembled enzyme as only one functional protein because the copies of the enzyme are all colocalized.

Bounded self-assembly can yield oscillations whose behavior is well-predicted by analytical formulae

The onset of oscillations for the bounded self-assembly system is well-predicted by two dimensionless parameters

We first consider a system where unphosphorylated kinase and phosphatase monomers self-assemble in an all-or-nothing manner into closed symmetric homomultimers. We denote by *n* the number of kinase monomers κ in the functional kinase multimer *K* and by *m* the analogous number of phosphatase monomers ρ in the multimer *P*. The reaction network is shown in Fig. 1B.

Since the full equations describing this bounded self-assembly system (eq. S1) are too complex to directly tackle analytically, we numerically integrate them within the parameter ranges outlined above (section S5). Our results, shown in Fig. 2, demonstrate a significant portion of parameter space within experimental constraints capable of admitting sustained oscillations.

To simplify these equations to an analytically tractable form, we make the Michaelis-Menten approximation that enzymatic intermediates are in quasi-steady state. We then make the approximation that the enzyme and substrate concentrations are low compared to the Michaelis constants, such that the concentration of enzymatic intermediates can be entirely neglected within our analytical approximations (section S2). This approximation, like others that we will consider, is not obeyed by all oscillating solutions found numerically (Fig. 2) but is nonetheless useful in clarifying the fundamentals of a large swath of the oscillations. We find that, in contrast to well-known examples from other systems that rely on enzyme sequestration to achieve oscillations (*6*, *7*), neglecting enzyme sequestration does not preclude oscillations for our systems.

To reduce our systems further to only two differential equations, we assume a separation of timescales between the self-assembly and the enzymatic activity. In particular, we assume that phosphorylation/dephosphorylation reactions equilibrate much faster than self-assembly. The opposite separation–of–timescales limit yields oscillations only for extremely large values of *m*, which are infeasible to realize

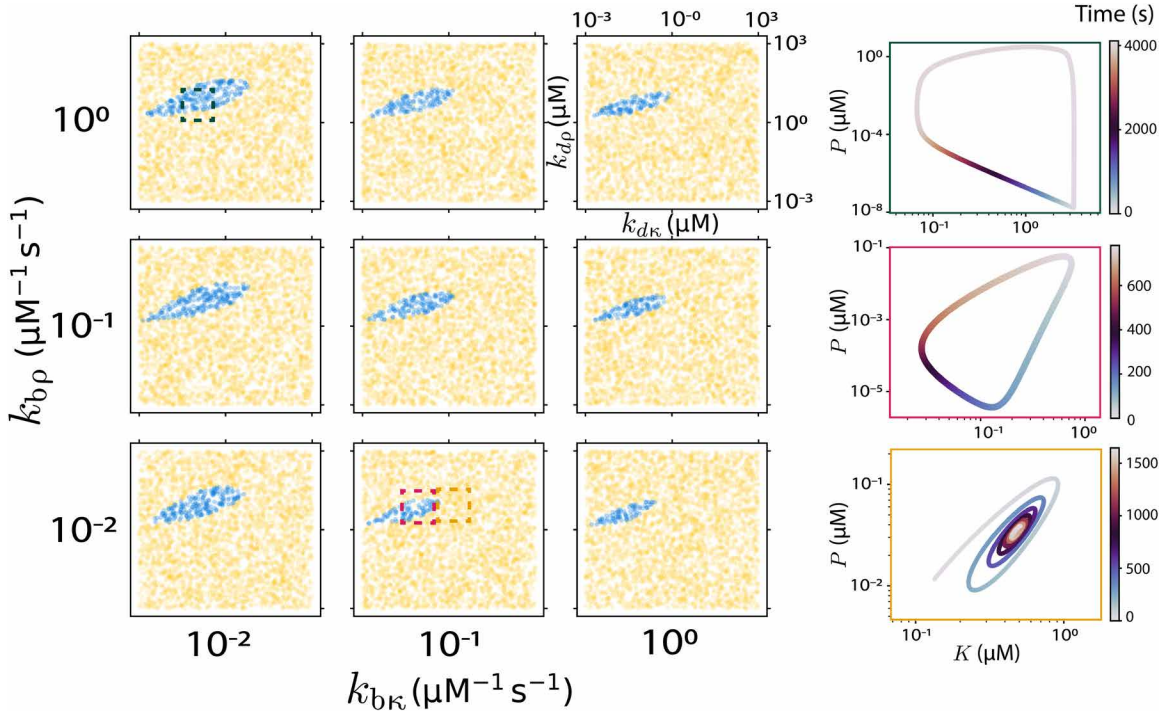

Fig. 2. Bounded self-assembly can yield oscillations using experimentally realizable parameters. Numerical integration of eq. S1 displays parameter regimes leading to oscillations within experimental constraints. Each subplot shows the location of oscillating parameter sets as a function of $k_{d\kappa}$ and $k_{d\rho}$ for given $k_{b\kappa}$ and $k_{b\rho}$; the latter two are varied for each subplot. Aside from experimental constraints (see main text for discussion), we set $n = m = 2$, $\kappa_{tot} = \rho_{tot} = 10$ μM, and $\widetilde{P}_{tot} = 10^{-4}$ μM. Blue points denote parameter sets leading to sustained oscillations; yellow points denote parameter sets leading to steady state. To the right of the plot, we show a few example trajectories in *K-P* phase space. The closed trajectories correspond to sustained oscillations; the final trajectory, the spiral, corresponds to a decaying oscillation and therefore to a yellow point in the figure.

experimentally (see further discussion in section S4). We thereby arrive at the following two-dimensional system of equations

$$\frac{dK}{dt} = k_{b\kappa}\left(\frac{\kappa_{tot} - nK}{1 + \eta_\kappa \frac{K}{P+\widetilde{P}}}\right)^n - k_{u\kappa}K$$
$$\frac{dP}{dt} = k_{b\rho}\left(\frac{\rho_{tot} - mP}{1 + \eta_\rho \frac{K}{P+\widetilde{P}}}\right)^m - k_{u\rho}P \quad (1)$$

We briefly define the parameters: $k_{b\kappa}$ is the binding rate for κ into its multimeric state, $k_{u\kappa}$ is the respective unbinding rate, and $k_{d\kappa}$ is the inverse ratio of the two; $\eta_{K\kappa}$ is the specificity constant k_{cat}/K_M for the kinase K acting on κ, $\eta_{P\kappa}$ is the same for the phosphatase P, and $\eta_\kappa = \eta_{K\kappa}/\eta_{P\kappa}$; κ_{tot} is the total concentration of monomeric κ added to the system, a conserved quantity. Similar quantities are defined for ρ. We assume the concentration of the constitutive phosphatase $\widetilde{P} > 0$ throughout (see section S2).

To describe the oscillatory behavior of the system, we seek the eigenvalues of the Jacobian in the vicinity of a fixed point $(K^\star, P^\star)$. Oscillations require coupling between the equations, motivating the approximations that in the oscillatory regime, $\eta_\kappa K^\star \gg P^\star + \widetilde{P}$ (and same for η_ρ), $\kappa_{tot} \gg nK^\star$, and $\rho_{tot} \gg mP^\star$. Defining the dimensionless concentrations $\widetilde{K^\star} = K^\star/\widetilde{P}$ and $\widetilde{P^\star} = P^\star/\widetilde{P}$, the fixed point in these limits is given by

$$\widetilde{P^\star}^{(n+1)} = \gamma\left(\widetilde{P^\star} + 1\right)^m$$
$$\widetilde{K^\star} = \alpha\,\widetilde{P^\star}^{(n/m)} \quad (2)$$

where γ and α are dimensionless parameters defined by

$$\gamma = \frac{k_{d\kappa}^m}{k_{d\rho}^{n+1}}\left(\frac{\eta_\kappa}{\kappa_{tot}}\right)^{nm}\left(\frac{\rho_{tot}}{\eta_\rho}\right)^{(n+1)m}\widetilde{P}^{(m-n-1)}$$
$$\alpha = \frac{k_{d\rho}^{n/m}}{k_{d\kappa}}\left(\frac{\eta_\rho\,\kappa_{tot}}{\eta_\kappa\,\rho_{tot}}\right)^n\widetilde{P}^{(n-m)/m} \quad (3)$$

We constrain ourselves to $m \le n + 1$ so that, within our approximations, there is no more than one physical fixed point in the system as long as $\widetilde{P} > 0$, simplifying our analysis. (When no solutions to Eq. 2 exist, our assumptions leading to it break down.)

Sustained oscillations in the system typically correspond to complex eigenvalues of the Jacobian with positive real parts. However, following the Poincaré-Bendixson theorem, as long as our system has a single fixed point, instability of the fixed point must imply oscillations even if they are beyond the linear regime. Translated into constraints on $P^\star$, instability of the fixed point corresponds to

$$\left(\frac{(m-1)\,k_{u\rho} - (n+1)\,k_{u\kappa}}{(n+1)\,k_{u\kappa} + k_{u\rho}}\right)\frac{P^\star}{\widetilde{P}} > 1 \quad (4)$$

We directly verify Eq. 4 in fig. S6.

We now proceed to express Eq. 4 only in terms of the input parameters. Because Eq. 2 cannot be solved for $P^\star$ for general n, m, we consider the approximation that $P^\star = \gamma^{1/(n+1-m)}\widetilde{P} \gg \widetilde{P}$, equivalent within the constraint $m < n + 1$ to $\gamma \gg 1$. This approximation is most accurate for small values of m, since fewer terms are neglected. The approximation is motivated by the intuition that oscillations require P to be non-negligible compared to $\widetilde{P}$; indeed, an opposite self-consistent solution, in which $P^\star \ll \widetilde{P}$, is incompatible with oscillations.

By simplifying Eq. 4 within this limit where $P^\star = \gamma^{1/(n+1-m)}\widetilde{P}$, we find that the system oscillates when

$$\nu \equiv \frac{(m-1)\,k_{u\rho}}{(n+1)\,k_{u\kappa}} > 1 \quad (5)$$

This corresponds to ensuring a positive left-hand side in Eq. 4 (see fig. S6).

The implication of Eq. 5, that oscillations require a larger dissociation rate of the phosphatase monomers compared to the kinase monomers (at least, for $n + 2 \ge m$), agrees with intuition found by visualizing individual oscillation cycles (Fig. 3A). In *K*-*P* space, oscillations proceed in a counterclockwise fashion: Starting from the unphosphorylated state, the monomers self-assemble into multimers (top right). The larger dissociation rate of phosphatase multimers leads those to dissociate first and get phosphorylated by the abundant kinase multimers (bottom right). Next, the kinase multimers slowly dissociate, enabling the gradual dephosphorylation and self-assembly of the phosphatase monomers by the constitutive and self-assembled phosphatases (bottom left). Once kinase multimer levels have decreased and enough phosphatase multimers have formed, the latter quickly dephosphorylate the remaining monomers (top left), and the system returns to its initial state (top right).

We verify that the approximate formula given by Eq. 5 is valid in describing Eq. 1 by comparing it to oscillations found by random parameter searches in Fig. 3B. We numerically integrate Eq. 1 with random parameters chosen to satisfy the experimental constraints described previously (including setting $\eta_\kappa = \eta_\rho$) and with $n = m = 2$. We constrain concentrations κ_{tot} and ρ_{tot} to be within 10^{-3} to 10^2 μM, while we set the bounds of $\widetilde{P}$ to 10^{-8} and 10^{-2} μM. For each parameter set, we numerically estimate the fixed point using Python's scipy.optimize.root function. We only show parameter sets estimated to agree with the approximations described before Eq. 2 (with >5× substituted for ≫). We found no oscillations in ~2.5×10^4 parameter sets for which η_K or η_P is less than $(P^\star + \widetilde{P})/K^\star$. Each blue (yellow) point in the figure corresponds to a single parameter set found to produce (not produce) oscillations starting from initial conditions of $(K, P) = (0,0)$. Oscillations are almost exclusively found in the quadrant $\gamma > 1$, $\nu > 1$. Values of γ slightly less than unity are also found to produce oscillations, as shown in the figure.

These results show that oscillations are found when the dissociation rate of the phosphatase multimer is in a middle range between two extremes. To see oscillations, the phosphatase multimer must dissociate significantly faster than the kinase multimer ($\nu > 1$); however, the dissociation rate must concurrently be small enough such that the fixed point concentration of phosphatase multimer is larger than the constitutive phosphatase concentration ($\gamma > 1$). In contrast to intuition from other systems, which signifies that higher-order nonlinearities increase the parameter range producing oscillations (*6*), here, we found that more nonlinear self-assembly (i.e., higher values of n and m) makes oscillations less frequent. We find that oscillations are robust to even order-of-magnitude variations in most other parameters (section S3 and fig. S2).

Our results suggest that oscillations in the concentrations of unphosphorylated monomers or of phosphatase multimers may be

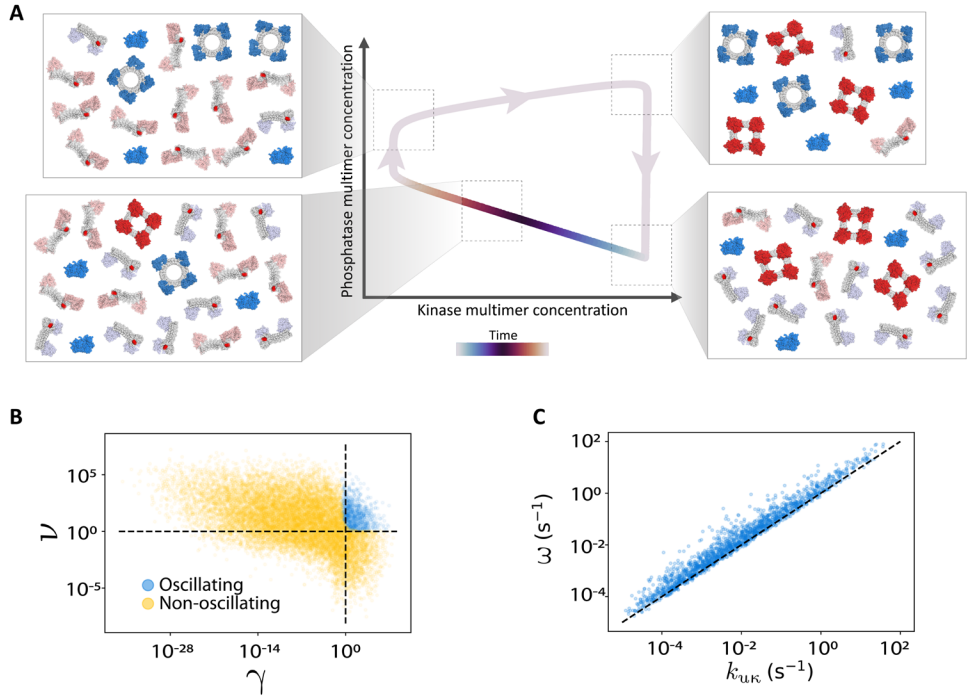

Fig. 3. Analytical results for bounded self-assembly oscillator. In this figure, we show results from the analytically simplified bounded self-assembly oscillator (Eq. 1), using $n = m = 2$. (**A**) Oscillation schematic. We visualize a sample oscillation using randomly and arbitrarily chosen parameters satisfying experimental constraints. Oscillations require phosphatase multimers (blue) to dissociate faster than kinase multimers (red). The system starts with self-assembled kinases and phosphatases (top right). After rapid phosphatase disassembly and phosphorylation by the kinase multimers (bottom right), the kinases slowly disassemble, which enables the gradual dephosphorylation and self-assembly of the phosphatase monomers (bottom left). The assembled phosphatases are then able to rapidly promote their own and kinase self-assembly through dephosphorylation, returning the system to its initial state (top right). (**B**) Onset of oscillations. Numerical integration demonstrates consistency with Eq. 5 for the appearance of oscillations in the appropriate limits. Each point represents a random set of parameters, sampled within the experimentally realizable limits as described in the main text. Oscillating (blue) and non-oscillating (yellow) parameter sets can be well-separated by dimensionless combinations of parameters γ and ν. Dashed lines show where the dimensionless parameters on the axes equal unity. (**C**) Oscillation frequency. Intuition from linear stability analysis of the fixed point suggests that for the $n = m = 2$ system considered numerically, oscillation frequency may be determined by the dissociation rate of kinase multimers, $k_{u\kappa}$. Numerical integration demonstrates that $k_{u\kappa}$ is indeed highly predictive of oscillation frequency ($R^2 \approx 0.66$; $R^2 \approx 0.93$ in log space) and underestimates the true frequency by a typical factor of ~4. Black dashed line shows $\omega = k_{u\kappa}$.

most straightforward to visualize experimentally, as these concentrations typically vary by several orders of magnitude across an oscillatory cycle (fig. S8). Parameter sets yielding largest oscillation amplitudes are also typically farthest from the bifurcation point (fig. S10).

The frequency of resulting oscillations can be well-predicted by assuming that kinase multimer dissociation is rate limiting

We next seek to predict how system parameters tune the frequency of resulting oscillations when they appear. Within the linear regime around the fixed point, in the limit of Eq. 5, the frequency of oscillations ω is predicted to be

$$\omega_{\text{pred}}^2 = -\frac{1}{4}[(n+1)\,k_{u\kappa} + (m-1)\,k_{u\rho}]^2 + nm\,k_{u\kappa}\,k_{u\rho} \qquad (6)$$

While Eq. 6 agrees well with the true squared frequency for those parameter sets where it is positive, oscillations are frequently found in the nonlinear regime in which it is not applicable (fig. S7A). However, the intuition given by Eq. 6, that oscillation frequency is determined by the unbinding rates of the kinase and phosphatase multimers, may still be valid outside the linear regime of the fixed point. This intuition is reasonable given the separation–of–timescales limit in which we are operating, of enzymatic reactions equilibrating much faster than self-assembly. Since oscillations for the $n = m = 2$ system that we considered numerically require that $k_{u\rho} > k_{u\kappa}$ (i.e., $\nu > 1$), Eq. 6 implies that the limiting reaction in the oscillations is the unbinding of the kinase multimers. To test that implication, we compare $k_{u\kappa}$ to the frequency of oscillations found through numerical integration in Fig. 3C. (We make no constraints on the fixed points of the parameter sets considered here.) We find a strong correlation ($R^2 = 0.66$; $R^2 = 0.93$ in log space) and a root mean square relative error of ~3.9, demonstrating that $k_{u\kappa}$ can accurately predict the frequency of oscillations in this system.

Oscillations found within experimental constraints for Eq. 1 have periods ranging from fractions of a second to >1 day (fig. S7B). For oscillations found for the full system of equations plotted in Fig. 2, we find periods within a slightly more constrained range than for the simplified system but still spanning orders of magnitude, between ~1 min and >1 day.

Unbounded self-assembly can yield oscillations within experimental constraints in the limit of fast self-assembly compared to enzymatic activity

We now consider a second system in which individual species κ and ρ can self-assemble incrementally into one-dimensional unbounded fibers (Fig. 4A). Unlike the bounded case in which no phosphorylation

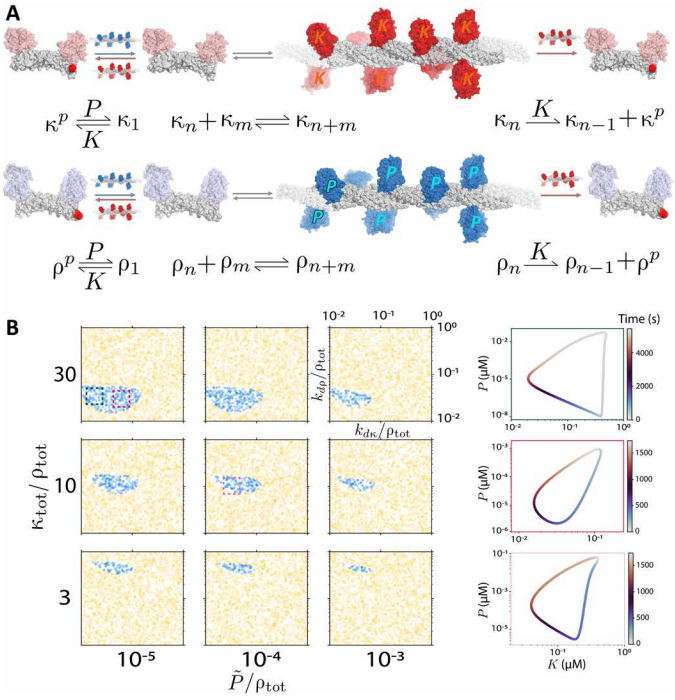

Fig. 4. Unbounded self-assembly oscillator. (**A**) Unbounded self-assembly reactions. We consider a related system to that shown in Fig. 1 but relying on kinase and phosphatase monomers that self-assemble into unbounded fibers of arbitrary length. In addition, we assume that the final monomer of each fiber can get phosphorylated by a kinase multimer, at which point it can no longer rejoin the fiber until it is dephosphorylated. (**B**) Unbounded self-assembly oscillations using experimentally realizable parameters. Numerical integration of Eq. 9 displays parameter regimes leading to oscillations within experimental constraints. Eq. 9 was used in place of the full system of equations (eq. S8) because of the infinite dimensionality of the latter. ρ_{tot} sets the concentration scale.

sites are accessible in the multimeric state, in this system, one is (corresponding to the final protein in the fiber). An n-mer of species X (where X is either κ or ρ), X_n, can be created either from binding two smaller molecules X_m and X_{n-m} or from the spontaneous breaking of a bond of a larger molecule. The concentration of X_n decreases when an X_n molecule either binds to any other molecule or breaks any of its $n-1$ bonds. The equations for self-assembly of species X are therefore given by

$$\frac{dX_n}{dt} = k_{bX}\left(\sum_{m=1}^{n-1} X_m X_{n-m} - 2X_n \sum_{m=1}^{\infty} X_m\right) + k_{uX}\left(2\sum_{m=n+1}^{\infty} X_m - (n-1)X_n\right) \quad (7)$$

As in the first system, each protein of type κ (ρ) includes a split kinase (phosphatase). While in the bounded system, enzymes required exactly n or m monomers to self-assemble, here, an enzyme is created by any group of more than one monomer (i.e., X_n is a functional enzyme as long as $n \geq 2$). We assume that when a multimer is phosphorylated, its final monomer dissociates from the fiber and cannot reassociate in its phosphorylated state. A less stringent assumption, that the phosphorylated monomer does not dissociate automatically but merely prevents new monomers from binding to that end of the molecule, appears to be incompatible with oscillations, at least in both separation–of–timescales limits.

The full equations describing the system are given in the Supplementary Materials (eq. S8). As previously, we search for a two-dimensional set of simplified equations by considering a separation of timescales between enzymatic reactions and self-assembly, along with the same simplifying assumptions as considered for the bounded self-assembly system (eq. S9). The limit considered for the first system, of fast phosphorylation/dephosphorylation compared to self-assembly, would disallow multimers from forming in this system, since, here, phosphorylation is accompanied by dissociation of the final multimer in the chain. Therefore, the separation–of–timescales limit considered in the bounded self-assembly system is no longer applicable for this system. Instead, we consider the opposite limit, of fast self-assembly compared to enzymatic activity. At steady state, X_n is given by

$$X_n = \frac{k_{uX}}{k_{bX}}\left(\frac{x}{1+x+\sqrt{1+2x}}\right)^n \quad (8)$$

where $x = 2k_{bX}X_{tot}/k_{uX} = 2X_{tot}/k_{dX}$. The same steady state is reached even if self-assembly involves binding and unbinding only a single monomer at a time.

The concentrations of phosphorylated monomers as a function of time are given by κ^p and ρ^p. The total amount of kinase present is given by $K = \Sigma_{i=2}^{\infty}\kappa_i$ and similarly for phosphatase. Since only the phosphorylation site of the final monomer in a multimer is exposed, the total number of available phosphorylation sites in the κ species is given by $\Sigma_{i=1}^{\infty}\kappa_i$ (and similarly for ρ). The system can be described by two differential equations for $k = 2(\kappa_{tot} - \kappa^p)/k_{d\kappa}$ and $p = 2(\rho_{tot} - \rho^p)/k_{d\rho}$

$$\begin{aligned}
\frac{dk}{dt} &= \frac{-2\eta_{K\kappa}k}{1+\sqrt{1+2k}}K + \eta_{P\kappa}\left(\frac{2\kappa_{tot}}{k_{d\kappa}} - k\right)(P+\tilde{P}) \\
\frac{dp}{dt} &= \frac{-2\eta_{K\rho}p}{1+\sqrt{1+2p}}K + \eta_{P\rho}\left(\frac{2\rho_{tot}}{k_{d\rho}} - p\right)(P+\tilde{P}) \\
K &= k_{d\kappa}\frac{k^2}{(1+\sqrt{1+2k})(1+k+\sqrt{1+2k})} \\
P &= k_{d\rho}\frac{p^2}{(1+\sqrt{1+2p})(1+p+\sqrt{1+2p})}
\end{aligned} \quad (9)$$

Unlike in the previous system for which the frequency and onset of oscillations can be determined by simple formulae by taking a limit of the two-dimensional system, no such limits give similarly straightforward results for Eq. 9. Instead, we analyze Eq. 9 through random parameter searches (Fig. 4B). As shown in the figure, we find that although these equations assume an opposite separation–of–timescales limit to that yielding experimentally realizable oscillations for the system of bounded self-assembly, they can nevertheless yield oscillations within a significant region of parameter space consistent with experimental constraints.

We find that increased values of κ_{tot}/ρ_{tot} and decreased values of $\tilde{P}/\rho_{tot}$ lead to more robust oscillations in this system; see fig. S3 for further discussion of oscillation robustness. The periods of oscillations found ranged from <1 min to >1 day (fig. S7B). Finally, we find that the concentrations of phosphatase multimers and unphosphorylated phosphatase monomers typically vary by several orders of magnitude across an oscillatory cycle (fig. S9), suggesting that oscillations may be most straightforward to visualize experimentally by measuring these concentrations.

DISCUSSION

In summary, we have presented two posttranslational protein–based oscillators motivated by the biological KaiABC system and by the synthetic dual-feedback genetic oscillator. Both systems that we present rely on split kinase and phosphatase self-assembling to form functional enzymes and on that self-assembly being inhibited by phosphorylation of the split monomers. The two systems differ mainly in the nature of the self-assembly as all-or-nothing into bounded structures of specified size or incremental into unbounded one-dimensional fibers.

Both systems are capable of producing oscillations within experimental constraints, using experimentally determined wild-type values for kinase and phosphatase activity and for a range of designed self-assembly rates. We have shown that neither complex reactions nor large number of species are necessary to achieve oscillations: Both networks that we present use only three protein species interacting only through reversible binding and phosphorylation/dephosphorylation reactions, and the resulting oscillations can be understood as arising from a minimal system of two differential equations in both cases.

Although the systems that we described shared much in common, they produced robust oscillations in opposite separation–of–timescales limits from one another: The first primarily oscillates when self-assembly is much slower than enzymatic reactions; the second when it is much faster. These two networks are thus complementary: Depending on the parameter regime most easily accessible to an experimentalist, one or the other network might be preferable to implement. Nevertheless, the conditions giving rise to oscillations shared similarities in the two systems. Smaller values of constitutive phosphatase (equivalent to larger values of γ in the case of bounded self-assembly) lead to more robust oscillations in both systems, as do smaller values of $k_{d\kappa}$ (i.e., larger values of ν).

Our work paves the way toward the rational design and experimental realization of protein-based far-from-equilibrium dynamic systems. The models described here were designed to be feasible to synthesize experimentally and are guiding an implementation in the test tube that is currently under way.

SUPPLEMENTARY MATERIALS

Supplementary material for this article is available at http://advances.sciencemag.org/cgi/content/full/6/51/eabc1939/DC1

View/request a protocol for this paper from *Bio-protocol*.

REFERENCES AND NOTES

1. O. Purcell, N. J. Savery, C. S. Grierson, M. di Bernardo, A comparative analysis of synthetic genetic oscillators. *J. R. Soc. Int.* **7**, 1503–1524 (2010).
2. M. W. Young, S. A. Kay, Time zones: A comparative genetics of circadian clocks. *Nat. Rev. Genet.* **2**, 702–715 (2001).
3. D. Bray, Protein molecules as computational elements in living cells. *Nature* **376**, 307–312 (1995).
4. X. J. Gao, L. S. Chong, M. S. Kim, M. B. Elowitz, Programmable protein circuits in living cells. *Science* **1258**, 1252–1258 (2018).
5. T. Fink, J. Lonzarić, A. Praznik, T. Plaper, E. Merljak, K. Leben, N. Jerala, T. Lebar, Ž. Strmšek, F. Lapenta, M. Benčina, R. Jerala, Design of fast proteolysis-based signaling and logic circuits in mammalian cells. *Nat. Chem. Biol.* **15**, 115–122 (2018).
6. B. Novák, J. J. Tyson, Design principles of biochemical oscillators. *Nat. Rev. Mol. Cell Biol.* **9**, 981–991 (2008).
7. C. C. Jolley, K. L. Ode, H. R. Ueda, A design principle for a posttranslational biochemical oscillator. *Cell Rep.* **2**, 938–950 (2012).
8. M. Nakajima, K. Imai, H. Ito, T. Nishiwaki, Y. Murayama, H. Iwasaki, T. Oyama, T. Kondo, Reconstitution of circadian oscillation of cyanobacterial KaiC phosphorylation in vitro. *Science* **308**, 414–415 (2005).
9. J. Michael, J. S. Markson, W. S. Lane, D. S. Fisher, E. K. O'Shea, Ordered phosphorylation governs oscillation of a three-protein circadian clock. *Science* **318**, 809–812 (2007).
10. M. J. Rust, Orderly wheels of the cyanobacterial clock. *Proc. Natl. Acad. Sci. U.S.A.* **109**, 16760–16761 (2012).
11. H. Kageyama, T. Nishiwaki, M. Nakajima, H. Iwasaki, T. Oyama, T. Kondo, Cyanobacterial circadian pacemaker: Kai protein complex dynamics in the KaiC phosphorylation cycle in vitro. *Mol. Cell* **23**, 161–171 (2006).
12. S. E. Boyken, M. A. Benhaim, F. Busch, M. Jia, M. J. Bick, H. Choi, J. C. Klima, Z. Chen, C. Walkey, A. Mileant, A. Sahasrabuddhe, K. Y. Wei, E. A. Hodge, S. Byron, A. Quijano-Rubio, B. Sankaran, N. P. King, J. Lippincott-Schwartz, V. H. Wysocki, K. K. Lee, D. Baker, De novo design of tunable, pH-driven conformational changes. *Science* **364**, 658–664 (2019).
13. B. Kholodenko, Negative feedback and ultrasensitivity can bring about oscillations in the mitogen-activated protein kinase cascades. *Eur. J. Biochem.* **267**, 1583–1588 (2000).
14. M. Strumillo, P. Beltrao, Towards the computational design of protein posttranslational regulation. *Bioorg. Med. Chem.* **23**, 2877–2882 (2015).
15. L. Doyle, J. Hallinan, J. Bolduc, F. Parmeggiani, D. Baker, B. L. Stoddard, P. Bradley, Rational design of α-helical tandem repeat proteins with closed architectures. *Nature* **528**, 585–588 (2015).
16. H. Nishi, K. Hashimoto, A. R. Panchenko, Phosphorylation in protein-protein binding: Effect on stability and function. *Structure* **19**, 1807–1815 (2011).
17. H. Nishi, A. Shaytan, A. R. Panchenko, Physicochemical mechanisms of protein regulation by phosphorylation. *Front. Genet.* **5**, 270 (2014).
18. K. Camacho-Soto, J. Castillo-Montoya, B. Tye, I. Ghosh, Ligand-gated split-kinases. *J. Am. Chem. Soc.* **136**, 3995–4002 (2014).
19. K. Camacho-Soto, J. Castillo-Montoya, B. Tye, L. O. Ogunleye, I. Ghosh, Small molecule gated split-tyrosine phosphatases and orthogonal split-tyrosine kinases. *J. Am. Chem. Soc.* **136**, 17078–17086 (2014).
20. Z. Li, S. Liu, Q. Yang, Incoherent inputs enhance the robustness of biological oscillators. *Cell Syst.* **5**, 72–81.e4 (2017).
21. P. Smolen, Frequency selectivity, multistability, and oscillations emerge from models of genetic regulatory systems. *Am. J. Physiol.* **274**, C531–C542 (1998).
22. J. Hasty, M. Dolnik, V. Rottschäfer, J. J. Collins, Synthetic gene network for entraining and amplifying cellular oscillations. *Phys. Rev. Lett.* **88**, 148101 (2002).
23. J. Stricker, S. Cookson, M. R. Bennett, W. H. Mather, L. S. Tsimring, J. Hasty, A fast, robust and tunable synthetic gene oscillator. *Nature* **456**, 516–519 (2008).
24. M. Schlosshauer, D. Baker, Realistic protein-protein association rates from a simple diffusional model neglecting long-range interactions, free energy barriers, and landscape ruggedness. *Protein Sci.* **13**, 1660–1669 (2004).
25. S. E. A. Ozbabacan, H. B. Engin, A. Gursoy, O. Keskin, Transient protein–protein interactions. *Protein Eng. Des. Sel.* **24**, 635–648 (2011).
26. S. Zhuo, J. C. Clemens, R. L. Stone, J. E. Dixon, Mutational analysis of a Ser/Thr phosphatase. *J. Biol. Chem.* **269**, 26234–26238 (1994).
27. C. Chen, B. H. Ha, A. F. Thévenin, H. J. Lou, R. Zhang, K. Y. Yip, J. R. Peterson, M. Gerstein, P. M. Kim, P. Filippakopoulos, S. Knapp, T. J. Boggon, B. E. Turk, Identification of a major determinant for serine-threonine kinase phosphoacceptor specificity. *Mol. Cell* **53**, 140–147 (2014).
28. R. A. Langan, S. E. Boyken, A. H. Ng, J. A. Samson, G. Dods, A. M. Westbrook, T. H. Nguyen, M. J. Lajoie, Z. Chen, S. Berger, V. K. Mulligan, J. E. Dueber, W. R. P. Novak, H. El-Samad, D. Baker, De novo design of bioactive protein switches. *Nature* **572**, 205–210 (2019).
29. A. H. Ng, T. H. Nguyen, M. Gómez-Schiavon, G. Dods, R. A. Langan, S. E. Boyken, J. A. Samson, L. M. Waldburger, J. E. Dueber, D. Baker, H. El-Samad, Modular and tunable biological feedback control using a de novo protein switch. *Nature* **572**, 265–269 (2019).

Acknowledgments: We thank A. Murugan for helpful discussions. **Funding:** This work was supported by the Harvard Materials Research Science and Engineering Center grant no. DMR-1420570 and ONR grant no. N00014-17-1-3029 (to M.P.B.). O.K. acknowledges funding from the DoD through NDSEG Fellowship 32 CFR 168a, the NSF-Simons Center for Mathematical and Statistical Analysis of Biology at Harvard University award no. 1764269, and the Harvard Quantitative Biology Initiative. A.C. is a recipient of the Human Frontier Science Program Long-Term Fellowship and a Washington Research Foundation Senior Fellow. M.P.B. is an investigator of the Simons Foundation. M.P.B. is a Research Scientist at Google Research. **Author contributions:** O.K., C.P.G., A.I.C., and M.P.B. designed and implemented the numerical analyses. O.K. and A.I.C. designed and performed the analytical analyses. A.C.,

N.B.W., and D.B. developed the experimental feasibility. O.K. and A.C. implemented the figures. All authors developed the oscillator designs, designed the figures, and wrote the paper. **Competing interests:** The authors declare that they have no competing interests. **Data and materials availability:** All data needed to evaluate the conclusions in the paper are present in the paper and/or the Supplementary Materials. The code used in this study is available at https://github.com/ofer-kimchi/protein-oscillator. Additional data related to this paper may be requested from the authors.

Submitted 10 April 2020
Accepted 3 November 2020
Published 16 December 2020
10.1126/sciadv.abc1939

Citation: O. Kimchi, C. P. Goodrich, A. Courbet, A. I. Curatolo, N. B. Woodall, D. Baker, M. P. Brenner, Self-assembly–based posttranslational protein oscillators. *Sci. Adv.* **6**, eabc1939 (2020).

ScienceAdvances

Self-assembly–based posttranslational protein oscillators

Ofer Kimchi, Carl P. Goodrich, Alexis Courbet, Agnese I. Curatolo, Nicholas B. Woodall, David Baker, and Michael P. Brenner

Sci. Adv. **6** (51), eabc1939. DOI: 10.1126/sciadv.abc1939

Science Advances (ISSN 2375-2548) is published by the American Association for the Advancement of Science. 1200 New York Avenue NW, Washington, DC 20005. The title *Science Advances* is a registered trademark of AAAS.

Science Advances
AAAS

advances.sciencemag.org/cgi/content/full/6/51/eabc1939/DC1

Supplementary Materials for

Self-assembly–based posttranslational protein oscillators

Ofer Kimchi*, Carl P. Goodrich, Alexis Courbet, Agnese I. Curatolo, Nicholas B. Woodall, David Baker, Michael P. Brenner

*Corresponding author. Email: okimchi@g.harvard.edu

Published 16 December 2020, *Sci. Adv.* **6**, eabc1939 (2020)
DOI: 10.1126/sciadv.abc1939

This PDF file includes:

Supplementary Material

S1 Other oscillation schemes attempted

Before trying self-assembly based oscillations, we tried implementing oscillations based on phosphorylations or binding events accompanying a conformational change in the molecule. Such conformational changes can be difficult to design, but the recently-published LOCKR system (*28, 29*) demonstrates one way in which binding can accompany a conformational change. We considered a molecule A which can be phosphorylated or bind to another molecule. We assume that when it is bound or phosphorylated, the molecule undergoes a conformational change; in the language of the LOCKR system, it opens. We assume that the rate of binding of any molecule to the closed state $A^\star$ can be smaller than the analogous binding rate to the open state, but no other asymmetries between the rates of analogous reactions are allowed. We did not make simplifying assumptions such as the Michaelis-Menten approximation when considering these systems.

We found oscillations are possible if A can bind, and thus sequester, free kinases (Fig. S1a). Oscillations are also possible if A can bind a separate "key" peptide b, which itself either binds free kinase (K) or phosphatase (P) molecules. Finally, oscillations can also be found if b, either alongside or instead of binding kinase or phosphatase, can itself get phosphorylated. We assume phosphorylated b is inert, except in that it can interact with phosphatase to get dephosphorylated (Fig. S1b). However, we found no evidence of possible oscillations within the experimental limits considered in this paper, after trying for each network 2×10^6 random parameter sets logarithmically distributed within the acceptable ranges.

For example, although experimentally realizable values of η_κ and η_ρ are near (slightly above) unity, we found no evidence of oscillations for the system shown in Fig. S1a with values of $\eta_\kappa =$

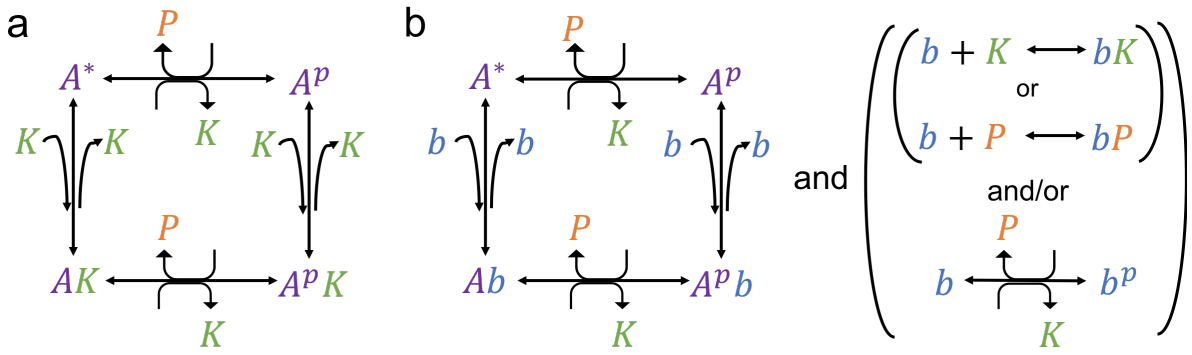

Figure S1: **Reaction networks giving oscillations outside of experimentally realizable regime.** See text for discussion.

η_ρ greater than 0.02, a difference of two orders of magnitude from the experimentally realizable regime. With future advances in protein engineering, the realm of experimental realizability may well expand and these networks may be able to yield *in vitro* oscillations. However, our work here is focused on those parameters that are currently reasonably accessible in the lab as described in the main text, and we therefore do not consider the networks shown in Fig. S1 further.

S2 Full kinetic equations and derivations of main text equations

Bounded self-assembly

We denote the concentration of phosphorylated (monomeric) κ by κ^p (and similarly for ρ). The concentration of the enzyme-substrate complex comprised of κ and K bound is denoted $\kappa \cdot K$. Binding, unbinding, and catalytic rate constants for the enzyme-substrate complexes are given by $k_{bK\kappa}, k_{uK\kappa}$, and $k_{cK\kappa}$, respectively. We use similar conventions for all other enzyme-substrate complexes. The full equations for the first system are:

$$
\begin{aligned}
\frac{d\kappa}{dt} &= -n(k_{b\kappa}\kappa^n + k_{u\kappa}K) - k_{bK\kappa}\kappa K + k_{uK\kappa}\kappa\cdot K + k_{cP\kappa}(\kappa^p\cdot P + \kappa^p\cdot\tilde{P})\\
\frac{d\rho}{dt} &= -m(k_{b\rho}\rho^m + k_{u\rho}P) - k_{bK\rho}\rho K + k_{uK\rho}\rho\cdot K + k_{cP\rho}(\rho^p\cdot P + \rho^p\cdot\tilde{P})\\
\frac{dK}{dt} &= k_{b\kappa}\kappa^n - k_{u\kappa}K - k_{bK\kappa}\kappa K + (k_{uK\kappa}+k_{cK\kappa})\kappa\cdot K - k_{bK\rho}\rho K + (k_{uK\rho}+k_{cK\rho})\rho\cdot K\\
\frac{dP}{dt} &= k_{b\rho}\rho^m - k_{u\rho}P - k_{bP\kappa}\kappa^p P + (k_{uP\kappa}+k_{cP\kappa})\kappa^p\cdot P - k_{bP\rho}\rho^p P + (k_{uP\rho}+k_{cP\rho})\rho\cdot P\\
\frac{d\kappa^p}{dt} &= -k_{bP\kappa}\kappa^p(P+\tilde{P}) + k_{uP\kappa}(\kappa^p\cdot P + \kappa^p\cdot\tilde{P}) + k_{cK\kappa}\kappa\cdot K\\
\frac{d\rho^p}{dt} &= -k_{bP\rho}\rho^p(P+\tilde{P}) + k_{uP\rho}(\rho^p\cdot P + \rho^p\cdot\tilde{P}) + k_{cK\rho}\rho\cdot K\\
\frac{d\kappa\cdot K}{dt} &= k_{bK\kappa}\kappa K - (k_{uK\kappa}+k_{cK\kappa})\kappa\cdot K\\
\frac{d\rho\cdot K}{dt} &= k_{bK\rho}\rho K - (k_{uK\rho}+k_{cK\rho})\rho\cdot K\\
\frac{d\kappa^p\cdot P}{dt} &= k_{bP\kappa}\kappa^p P - (k_{uP\kappa}+k_{cP\kappa})\kappa^p\cdot P\\
\frac{d\rho^p\cdot P}{dt} &= k_{bP\rho}\rho^p P - (k_{uP\rho}+k_{cP\rho})\rho^p\cdot P\\
\frac{d\kappa^p\cdot\tilde{P}}{dt} &= k_{bP\kappa}\kappa^p\tilde{P} - (k_{uP\kappa}+k_{cP\kappa})\kappa^p\cdot\tilde{P}\\
\frac{d\rho^p\cdot\tilde{P}}{dt} &= k_{bP\rho}\rho^p\tilde{P} - (k_{uP\rho}+k_{cP\rho})\rho^p\cdot\tilde{P}\\
\frac{d\tilde{P}}{dt} &= -k_{bP\kappa}\kappa^p\tilde{P} + (k_{uP\kappa}+k_{cP\kappa})\kappa^p\cdot\tilde{P} - k_{bP\rho}\rho^p\tilde{P} + (k_{uP\rho}+k_{cP\rho})\rho\cdot\tilde{P}.
\end{aligned}
\tag{S1}
$$

Making only the Michaelis-Menten approximation for enzymatic reactions and accounting for conservation laws, the equations can be reduced to the following four-dimensional system of equations:

$$
\begin{aligned}
\frac{dK}{dt} &= k_{b\kappa}\kappa^n - k_{u\kappa}K \\
\frac{dP}{dt} &= k_{b\rho}\rho^m - k_{u\rho}P \\
\frac{d\kappa}{dt} &= -n(k_{b\kappa}\kappa^n - k_{u\kappa}K) - \eta_{K\kappa}\kappa K + \eta_{P\kappa}\kappa^p(P+\tilde{P}) \\
\frac{d\rho}{dt} &= -m(k_{b\rho}\rho^m - k_{u\rho}P) - \eta_{K\rho}\rho K + \eta_{P\rho}\rho^p(P+\tilde{P}) \\
\kappa_{\text{tot}} &= \kappa + \kappa^p + nK + (n+1)\frac{\kappa K}{K_{M_{K\kappa}}} + \frac{\kappa^p(P+\tilde{P})}{K_{M_{P\kappa}}} + n\frac{\rho K}{K_{M_{K\rho}}} \\
\rho_{\text{tot}} &= \rho + \rho^p + mP + \frac{\rho K}{K_{M_{K\rho}}} + (m+1)\frac{\rho^p P}{K_{M_{P\rho}}} + \frac{\rho^p \tilde{P}}{K_{M_{P\rho}}} + m\frac{\kappa^p P}{K_{M_{P\kappa}}}
\end{aligned}
\tag{S2}
$$

where as in the main text, $\eta_{K\kappa}$ is the specificity constant $k_{cK\kappa}k_{bK\kappa}/(k_{uK\kappa} + k_{cK\kappa}) = k_{cK\kappa}/K_{M_{K\kappa}}$, and similar constants are similarly defined for other reactions.

In order to reduce our system further to only two differential equations, we assume a separation of timescales between the self-assembly and the enzymatic activity. In particular, we assume that phosphorylation/dephosphorylation reactions equilibrate much faster than self-assembly; see Section S4 for consideration of the opposite limit. Within the Michaelis-Menten approximation, this can be written as:

$$
\begin{aligned}
\eta_{K\kappa}\kappa K &= \eta_{P\kappa}\kappa^p(P+\tilde{P}) \\
\eta_{K\rho}\rho K &= \eta_{P\rho}\rho^p(P+\tilde{P})
\end{aligned}
\tag{S3}
$$

Making the approximation that the Michaelis constants are large compared to concentrations of the various components (such that $\kappa_{\text{tot}} = \kappa + \kappa^p + nK$, and likewise for ρ_{tot}) we arrive at

$$
\begin{aligned}
\kappa &= \frac{\kappa_{\text{tot}} - nK}{1 + \eta_\kappa \frac{K}{P+\tilde{P}}} \\
\rho &= \frac{\rho_{\text{tot}} - mP}{1 + \eta_\rho \frac{K}{P+\tilde{P}}}
\end{aligned}
\tag{S4}
$$

which, in conjunction with Eqn. S2, leads to Eqn. 1.

Bounded self-assembly: Evaluating the trace of the Jacobian

In order to derive Eqn. 4, we start by computing the Jacobian of Eqn. 1 and taking its trace. The trace can then be simplified by making the same approximations made to arrive at Eqn. 2 (namely, that $\eta_\kappa K^\star \gg P^\star + \tilde{P}$, $\eta_\rho K^\star \gg P^\star + \tilde{P}$, $\kappa_{\text{tot}} \gg nK^\star$, and $\rho_{\text{tot}} \gg mP^\star$). It is useful at this point to use Eqn. 2 to express the trace entirely in terms of $P^\star$.

$$\begin{aligned}\text{tr}(J) =& \frac{k_{d\kappa}}{\eta_\rho} k_{u\rho} m P^\star \rho_{\text{tot}} \left(\frac{\eta_\kappa \rho_{\text{tot}}}{\eta_\rho \kappa_{\text{tot}}}\right)^n (k_{d\rho} P^\star)^{-\frac{n+1}{m}} - \\ & \left(\frac{k_{b\kappa} n^2 k_{d\rho}^{\frac{n}{m}} P^{\star(n/m)} \left(\frac{\eta_\rho \kappa_{\text{tot}}}{\eta_\kappa \rho_{\text{tot}}}\right)^n}{\kappa_{\text{tot}}} + (n+1)k_{u\kappa} + \frac{k_{u\rho} m^2 P^\star}{\rho_{\text{tot}}} + k_{u\rho}\right).\end{aligned} \tag{S5}$$

We now replace the factors of $P^{\star\left(-\frac{n+1}{m}\right)}$ and $P^{\star(n/m)}$ with their appropriate expressions given Eqn. 2, getting a far cleaner expression:

$$\text{tr}(J) = -(n+1)k_{u\kappa} - n^2 k_{u\kappa}\frac{K^\star}{\kappa_{\text{tot}}} - k_{u\rho} + m k_{u\rho}\left(\frac{P^\star}{P^\star + \tilde{P}} - m\frac{P^\star}{\rho_{\text{tot}}}\right). \tag{S6}$$

After factoring out $nk_{u\kappa}$, we can rely on the approximations made previously that $\kappa_{\text{tot}} \gg nK^\star$, and $\rho_{\text{tot}} \gg mP^\star$ to neglect the second and final terms, leading to

$$\text{tr}(J) = -(n+1)k_{u\kappa} - k_{u\rho} + m k_{u\rho}\frac{P^\star}{P^\star + \tilde{P}} \tag{S7}$$

which we set greater than zero to arrive at Eqn. 4.

The $\tilde{P} = 0$ case

Eqns. S2 demonstrate that if $\tilde{P} = 0$, a new fixed point appears at $\kappa = \rho = K = P = 0$. The Jacobian at that fixed point has two negative and two zero eigenvalues. We find no evidence of oscillations in Eqns. S1 with $\tilde{P} = 0$ in 5×10^4 random parameter sets, nor do we find any oscillations when plotting the analogue of Fig. 2 for the case of $\tilde{P} = 0$.

Intuitively, if a system has no constitutive phosphatase activity, then if any fluctuation brings the total number of dephosphorylated ρ monomers to a value less than m, no recovery of phosphorylation activity is possible. In the presence of constitutive phosphatase, this is no longer true, leading to oscillation robustness. We therefore assume $\tilde{P} > 0$ throughout the manuscript.

Unbounded self-assembly

The full equations describing the second system are:

$$
\begin{aligned}
\frac{d\kappa_n}{dt} &= k_{b\kappa}\left(\sum_{m=1}^{n-1}\kappa_m\kappa_{n-m} - 2\kappa_n\sum_{m=1}^{\infty}\kappa_m\right) + k_{u\kappa}\left(2\sum_{m=n+1}^{\infty}\kappa_m - (n-1)\kappa_n\right) \\
&\quad + \sum_{m=2}^{\infty}\left(k_{cK\kappa}\kappa_{n+1}\cdot\kappa_m - k_{bK\kappa}\kappa_n\kappa_m + k_{uK\kappa}\kappa_n\cdot\kappa_m\right) + \delta_{n,1}k_{cP\kappa}\left(\kappa^p\cdot\tilde{P} + \sum_{m=2}^{\infty}\kappa^p\cdot\rho_m\right) \\
\frac{d\rho_n}{dt} &= k_{b\rho}\left(\sum_{m=1}^{n-1}\rho_m\rho_{n-m} - 2\rho_n\sum_{m=1}^{\infty}\rho_m\right) + k_{u\rho}\left(2\sum_{m=n+1}^{\infty}\rho_m - (n-1)\rho_n\right) \\
&\quad + \sum_{m=2}^{\infty}\left(k_{cK\rho}\rho_{n+1}\cdot\kappa_m - k_{bK\rho}\rho_n\kappa_m + k_{uK\rho}\rho_n\cdot\kappa_m\right) + \delta_{n,1}k_{cP\rho}\left(\rho^p\cdot\tilde{P} + \sum_{m=2}^{\infty}\rho^p\cdot\rho_m\right) \\
\frac{d\tilde{P}}{dt} &= -k_{bP\kappa}\kappa^p\tilde{P} + (k_{uP\kappa}+k_{cP\kappa})\kappa^p\cdot\tilde{P} - k_{bP\rho}\rho^p\tilde{P} + (k_{uP\rho}+k_{cP\rho})\rho^p\cdot\tilde{P} \\
\frac{d\kappa^p}{dt} &= k_{cK\kappa}\sum_{n=1}^{\infty}\sum_{m=2}^{\infty}\kappa_n\cdot\kappa_m - k_{bP\kappa}\kappa^p\left(\tilde{P} + \sum_{m=2}^{\infty}\rho_m\right) + k_{uP\kappa}\left(\kappa^p\cdot\tilde{P} + \sum_{m=2}^{\infty}\kappa^p\cdot\rho_m\right) \\
\frac{d\rho^p}{dt} &= k_{cK\rho}\sum_{n=1}^{\infty}\sum_{m=2}^{\infty}\rho_n\cdot\kappa_m - k_{bP\rho}\rho^p\left(\tilde{P} + \sum_{m=2}^{\infty}\rho_m\right) + k_{uP\rho}\left(\rho^p\cdot\tilde{P} + \sum_{m=2}^{\infty}\rho^p\cdot\rho_m\right) \\
\frac{d\kappa_n\cdot\kappa_m}{dt} &= k_{bK\kappa}\kappa_n\kappa_m - (k_{uK\kappa}+k_{cK\kappa})\kappa_n\cdot\kappa_m \\
\frac{d\rho_n\cdot\kappa_m}{dt} &= k_{bK\kappa}\kappa_n\kappa_m - (k_{uK\kappa}+k_{cK\kappa})\kappa_n\cdot\kappa_m \\
\frac{d\kappa^p\cdot\rho_m}{dt} &= k_{bP\kappa}\kappa^p\rho_m - (k_{uP\kappa}+k_{cP\kappa})\kappa^p\cdot\rho_m \\
\frac{d\kappa^p\cdot\tilde{P}}{dt} &= k_{bP\kappa}\kappa^p\tilde{P} - (k_{uP\kappa}+k_{cP\kappa})\kappa^p\cdot\tilde{P} \\
\frac{d\rho^p\cdot\rho_m}{dt} &= k_{bP\rho}\rho^p\rho_m - (k_{uP\rho}+k_{cP\rho})\rho^p\cdot\rho_m \\
\frac{d\rho^p\cdot\tilde{P}}{dt} &= k_{bP\rho}\rho^p\tilde{P} - (k_{uP\rho}+k_{cP\rho})\rho^p\cdot\tilde{P}.
\end{aligned}
\tag{S8}
$$

Within the Michaelis-Menten approximation and after accounting for conservation laws, these equations become:

$$
\begin{aligned}
\frac{d\kappa_n}{dt} &= k_{b\kappa}\left(\sum_{m=1}^{n-1}\kappa_m\kappa_{n-m} - 2\kappa_n\sum_{m=1}^{\infty}\kappa_m\right) + k_{u\kappa}\left(2\sum_{m=n+1}^{\infty}\kappa_m - (n-1)\kappa_n\right) \\
&\quad + \eta_{K\kappa}(\kappa_{n+1}-\kappa_n)K + \delta_{n,1}\eta_{P\kappa}\kappa^p(P+\tilde{P}) \\
\frac{d\rho_n}{dt} &= k_{b\rho}\left(\sum_{m=1}^{n-1}\rho_m\rho_{n-m} - 2\rho_n\sum_{m=1}^{\infty}\rho_m\right) + k_{u\rho}\left(2\sum_{m=n+1}^{\infty}\rho_m - (n-1)\rho_n\right) \\
&\quad + \eta_{K\rho}(\rho_{n+1}-\rho_n)K + \delta_{n,1}\eta_{P\rho}\rho^p(P+\tilde{P}) \\
K &= \sum_{n=2}^{\infty}\kappa_n; \quad P = \sum_{n=2}^{\infty}\rho_n \\
\kappa_{\text{tot}} &= \kappa^p + \sum_{n=1}^{\infty}n\kappa_n + \sum_{n=2}^{\infty}\kappa_n\sum_{m=1}^{\infty}\left(\frac{(n+m)\kappa_m}{K_{M_{K\kappa}}} + \frac{n\rho_m}{K_{M_{K\rho}}}\right) + \frac{\kappa^p(P+\tilde{P})}{K_{M_{P\kappa}}} \\
\rho_{\text{tot}} &= \rho^p + \sum_{n=1}^{\infty}n\rho_n + \sum_{n=2}^{\infty}\kappa_n\sum_{m=1}^{\infty}\frac{m\rho_m}{K_{M_{K\rho}}} + \sum_{n=2}^{\infty}\rho_n\left(\frac{n\kappa^p}{K_{M_{P\kappa}}} + \frac{(n+1)\rho^p}{K_{M_{P\rho}}}\right) + \frac{\rho^p\tilde{P}}{K_{M_{P\rho}}}.
\end{aligned}
\tag{S9}
$$

In order to arrive at Eqn. 9, we assume a separation of timescales between the self-assembly and the enzymatic activity. In particular, we assume that self-assembly reactions equilibrate much faster than phosphorylation/dephosphorylation. This is the opposite separation-of-timescales limit to that considered in the bounded self-assembly case. The reason we consider this limit here is that the limit of fast enzymatic activity compared to self-assembly (the limit considered for the bounded system) would result in any multimers immediately being broken up into monomers, since phosphorylation in this system is accompanied by the final monomer in the chain dissociating from the multimer.

We can then write the dynamics of the system only in terms of the phosphorylated monomers κ^p and ρ^p.

$$
\begin{aligned}
\frac{d\kappa^p}{dt} &= \eta_{K\kappa}\sum_{n=1}^{\infty}\kappa_n K - \eta_{P\kappa}\kappa^p(P+\tilde{P}) \\
\frac{d\rho^p}{dt} &= \eta_{K\rho}\sum_{n=1}^{\infty}\rho_n K - \eta_{P\rho}\rho^p(P+\tilde{P})
\end{aligned}
\tag{S10}
$$

where K and P are as defined in Eqn. 9. Writing these equations in terms of $k = 2(\kappa_{\text{tot}} - \kappa^p)/k_{d\kappa}$ and $p = 2(\rho_{\text{tot}} - \rho^p)/k_{d\rho}$, we arrive at Eqn. 9.

S3 Robustness analysis

Here we describe the robustness of oscillations to errors in parameter estimation. For example, while we may design experiments towards a particular value of each parameter, will oscillations disappear if our estimates of the parameters are slightly inaccurate? In order to address this question, we performed case studies of a random and arbitrarily chosen parameter set for both the bounded and unbounded self-assembly systems (Figs. S2 and S3, respectively). In particular, we used the first parameter set found using random sampling to yield oscillations. We then varied the parameters one by one, keeping all other parameters fixed, and measured the effects of these parameter variations on the presence and period of oscillations. Yellow points represent values of the parameter for which the system does not exhibit sustained oscillations; blue curves represent how the period of oscillation changes as a result of parameter variation.

For the bounded self-assembly system, we find that with the exception of the concentrations κ_{tot} and ρ_{tot}, oscillations are robust to even an order-of-magnitude error in parameter estimation. In addition, oscillations are robust to approximately 5-fold errors in κ_{tot} or ρ_{tot}. We also find that arbitrarily small values of $\tilde{P}$ can yield oscillations. Finally, as expected from the main text discussion, variations in $k_{u\kappa}$ most strongly affect the periods of resulting oscillations. We verify that are results are not dependent on the small values of $k_{u\kappa}$ and $k_{u\rho}$ in the randomly chosen parameter set, by performing the same analysis on a second random parameter set (Fig. S2b).

For the unbounded self-assembly system, we find that oscillations are less robust to parameter variation in two random and arbitrarily chosen parameter sets. One exception is the parameter $k_{d\kappa}$ which was found in the second parameter set to be variable by nearly two orders of magnitude in the oscillatory regime. Our results suggest oscillations may be more robust in the bounded self-assembly system than in the unbounded system.

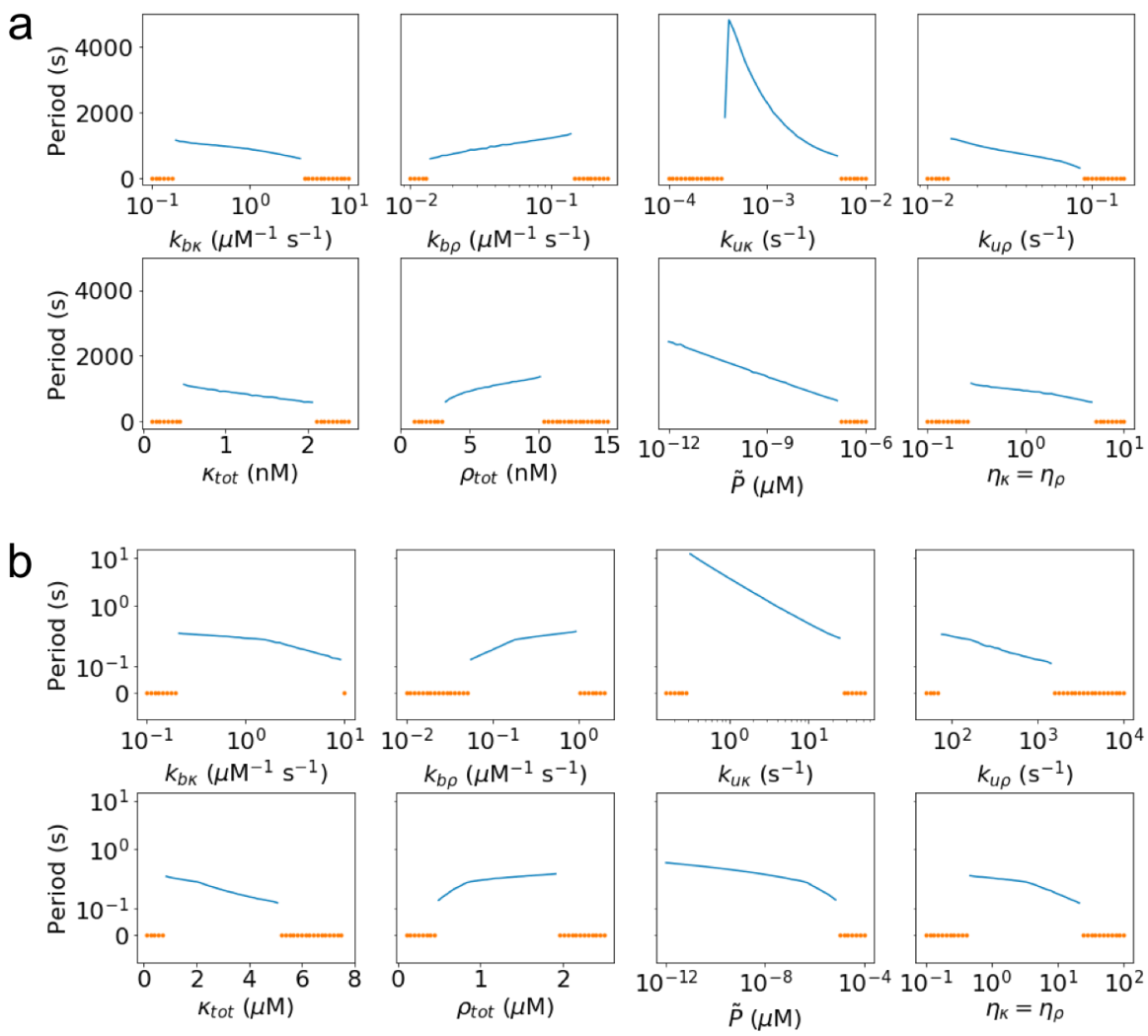

Figure S2: **Robustness analysis for bounded self-assembly system in the limit of fast enzymatic activity compared to self-assembly.** We consider the robustness of oscillations found for Eqn. 1. Yellow points represent values of the parameter for which the system does not exhibit sustained oscillations; blue curves represent how the period of oscillation changes as a result of parameter variation. Panel **a** uses the first oscillatory parameter set found. In order to verify that robustness of oscillations is not due to small values of $k_{u\kappa}$ and $k_{u\rho}$, panel **b** uses the first oscillatory parameter set found for which those values were both greater than 1 s^{-1}. In both parameter sets, oscillations are robust to over an order-of-magnitude variation in all parameters other than κ_{tot} and ρ_{tot}. All x-axes are in log-scale except for those two parameters. Arbitrarily small values of $\tilde{P}$ also give oscillations in both parameter sets. Finally, the period is heavily affected by $k_{u\kappa}$ as described in the main text.

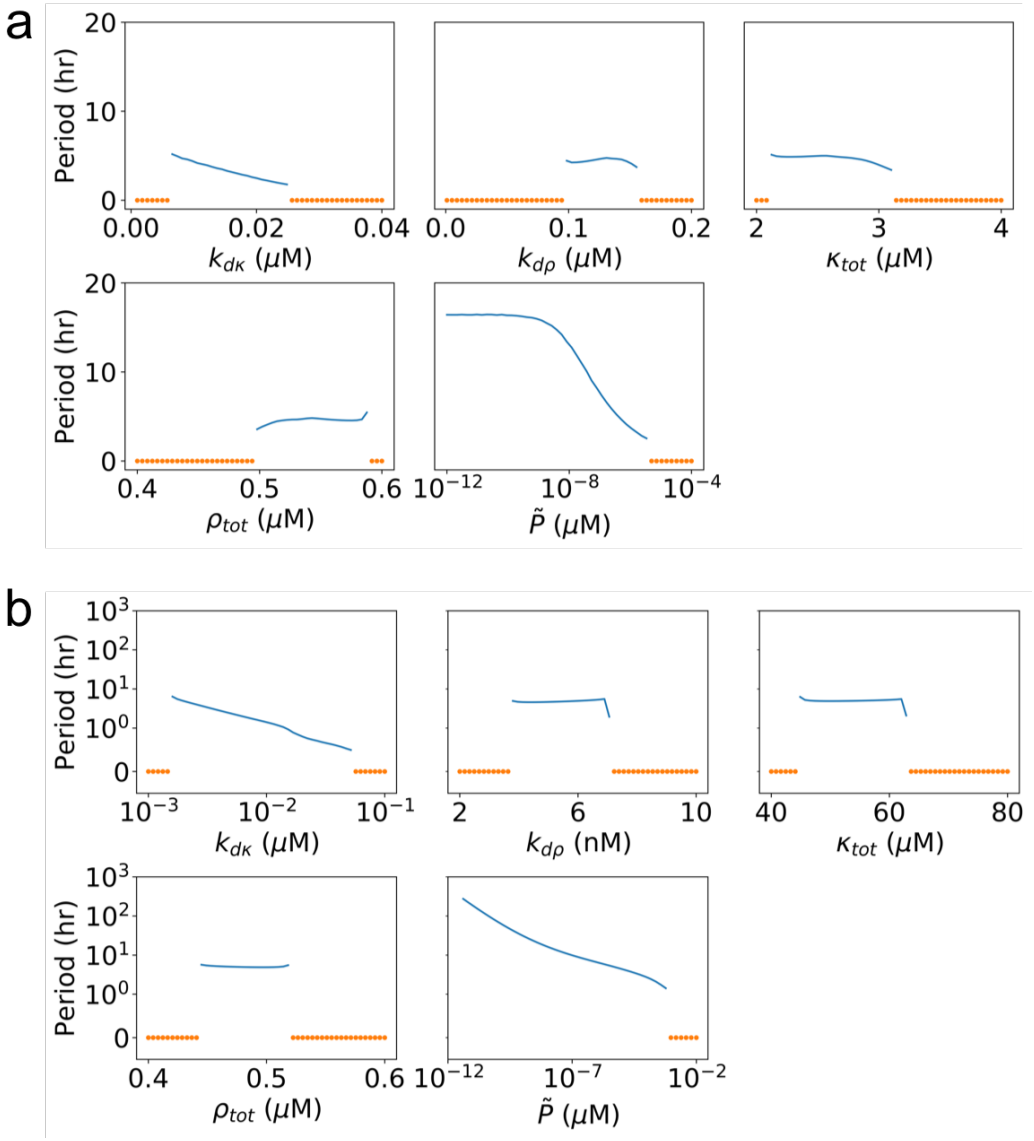

Figure S3: **Robustness analysis for unbounded self-assembly system.** We consider the robustness of oscillations found for Eqn. 9. Yellow points represent values of the parameter for which the system does not exhibit sustained oscillations; blue curve represents how the period of oscillation changes as a result of parameter variation. Panels **a** and **b** use the first two oscillatory parameter sets found. Oscillations appear less robust to parameter variations than in the bounded self-assembly system (Fig. S2), with the exception of the parameter $k_{d\kappa}$ in the second parameter set which can vary by nearly two orders of magnitude in the oscillatory regime. In addition, as in Fig. S2, arbitrarily small values of $\tilde{P}$ also give oscillations in both parameter sets.

S4 Considering the limit of fast self-assembly compared to enzymatic activity in the bounded self-assembly system

In the bounded self-assembly system, the limit corresponding to fast self-assembly compared to phosphorylation/dephosphorylation corresponds to the assumption

$$\begin{aligned} k_{b\kappa}\kappa^n &= k_{u\kappa}K \\ k_{b\rho}\rho^m &= k_{u\rho}P \end{aligned} \tag{S11}$$

Using this assumption, we can describe the system dynamics using a set of two coupled differential equations. Defining $k_{d\kappa} = k_{u\kappa}/k_{b\kappa}$, and similarly for ρ

$$\begin{aligned} \frac{d\kappa}{dt} &= -\eta_{K\kappa}\frac{\kappa^{n+1}}{k_{d\kappa}} + \eta_{P\kappa}\left(\kappa_{\text{tot}} - \kappa - n\frac{\kappa^n}{k_{d\kappa}}\right)\left(\frac{\rho^m}{k_{d\rho}} + \tilde{P}\right) \\ \frac{d\rho}{dt} &= -\eta_{K\rho}\rho\frac{\kappa^n}{k_{d\kappa}} + \eta_{P\rho}\left(\rho_{\text{tot}} - \rho - m\frac{\rho^m}{k_{d\rho}}\right)\left(\frac{\rho^m}{k_{d\rho}} + \tilde{P}\right). \end{aligned} \tag{S12}$$

Our goal is to determine whether this system can give rise to oscillations. Oscillations necessitate positive real parts of the Jacobian of the system evaluated at the fixed point, corresponding to positive values of its trace. The trace of the Jacobian is given by

$$\begin{aligned} \text{tr}(J) =& \frac{\partial\dot{\kappa}}{\partial\kappa} + \frac{\partial\dot{\rho}}{\partial\rho} \\ =& -\eta_{K\kappa}(n+1)\frac{\kappa^n}{k_{d\kappa}} - \eta_{P\kappa}\left(\frac{\rho^m}{k_{d\rho}} + \tilde{P}\right)\left(n^2\frac{\kappa^{n-1}}{k_{d\kappa}} + 1\right) \\ & - \eta_{K\rho}\frac{\kappa^n}{k_{d\kappa}} - \eta_{P\rho}\left((m+1)\frac{\rho^m}{k_{d\rho}} + \tilde{P} + \frac{2}{\rho}\left(\frac{m\rho^m}{k_{d\rho}}\right)^2 + m^2\frac{\rho^{m-1}}{k_{d\rho}}\tilde{P} - m\frac{\rho^{m-1}}{k_{d\rho}}\rho_{\text{tot}}\right). \end{aligned} \tag{S13}$$

where here and in the rest of the section, all concentrations are measured at the fixed point of Eqn. S12.

All terms in the trace are negative except for the last. Therefore, the system has the potential to oscillate only if the final term is larger in magnitude than all the rest combined.

To simplify, we notice that given our experimental constraints that $\eta_{K\kappa} = \eta_{K\rho}$ and $\eta_{P\kappa} = \eta_{P\rho}$, the following holds at the fixed point of Eqn. S12:

$$\frac{\eta_{K\rho}}{\eta_{P\rho}} \frac{K}{P + \tilde{P}} = \frac{\kappa^p}{\kappa} = \frac{\rho^p}{\rho}. \tag{S14}$$

Using these equalities and substituting in Eqn. S11 as well as the conservation law $\rho_{\text{tot}} = \rho^p + \rho + mP$, we find after some algebra that

$$\text{tr}(J) = -\eta_{K\rho} K \left(-m \frac{P}{P + \tilde{P}} + 2 + n + n^2 \frac{K}{\kappa^p} + 2\frac{\kappa}{\kappa^p} + m^2 \frac{P}{\rho^p} \right). \tag{S15}$$

In this form, it is clear that oscillations are not possible if $m < n + 3$. Oscillations are also not possible if the fixed point concentration of self-assembled phosphatase is not much larger than the concentration of constitutive phosphatase. However, this equation does not rule out oscillations for large values of m. We proceed by searching for oscillations numerically.

As in our other numerical studies in this work, we logarithmically sample random parameters. However, here, we also allow m to vary, as a randomly (uniformly) chosen integer between 5 and 20, while maintaining $n = 2$. We set the total concentrations of monomers to be between 10^{-4} and 100 μM and allow $\tilde{P}$ to vary between $10^{-6}/m$ μM and $\rho_{\text{tot}}/10m$. For this numerical study, we rescale time by a factor of $\eta_{K\rho} \times \mu$M. We choose values of k_d between 10^{-5} and 10^5 μM^{m-1}. We integrate each parameter set up to time 10^5 in rescaled time units; we found that 100 random parameter sets all reached steady state within a tenth of that time.

We examined 2×10^6 parameter sets randomly sampled in this fashion, and found 10 sets yielding oscillations for Eqn. S12. For comparison, we found 1717 out of 5×10^4 parameter sets yielding oscillations for Eqn. 1. The parameter sets yielding oscillations are given in Table S1. All oscillation periods found were far from 10^4, demonstrating that our integration time limit did not play a role in limiting oscillations found. The oscillating parameter sets found require extremely large values of m, beyond what is currently readily accessible experimentally. We

Index	n	m	η	$k_{d\kappa}$ (μM)	$k_{d\rho}$ (μM^{m-1})	κ_{tot} (μM)	ρ_{tot} (μM)	$\tilde{P}$ (μM)	Period
1	2	14	1.1	41.5	201	36.1	9.23	0.0591	5.82
2	2	12	1.1	68.8	0.0235	42.8	4.80	0.0309	17.0
3	2	17	1.1	979	11800	58.7	6.94	0.0322	12.8
4	2	15	1.1	399	0.00540	56.7	3.82	0.0193	40.3
5	2	9	1.1	124	5.15	96.3	9.11	0.0391	18.4
6	2	10	1.1	21.6	3.89e-5	50.5	3.75	0.0292	5.50
7	2	10	1.1	1090	2.60e-5	49.9	1.37	0.00710	56.8
8	2	20	1.1	26.4	0.434	56.5	10.6	0.0516	4.3
9	2	14	1.1	626	4.99e-4	32.7	2.20	0.0104	85.9
10	2	9	1.1	36.6	0.00308	85.6	5.92	0.0315	6.05

Table S1: Parameter sets found to yield oscillations in Eqn. S12, of 2×10^6 examined. The period is measured in the rescaled time units described in the main text.

analyze the robustness of the oscillations to one-dimensional variations in parameters in Fig. S4. Given the relative paucity of oscillating solutions found by random sampling and their apparent relative fragility (compared to Fig. S2) as well as the technical difficulties associated with implementing these solutions in the lab (in particular, with achieving robust homomultimeric self-assembly with large numbers of monomers per multimer), the limit of fast self-assembly compared to enzymatic activity appears less promising than the opposite limit considered in the main text of this work.

We do not consider here hybrid systems where the kinase self-assembly is bounded while the phosphatase is unbounded (or vice versa) though this analysis suggests that in the limit of fast self-assembly, such systems may be worth examining in greater detail.

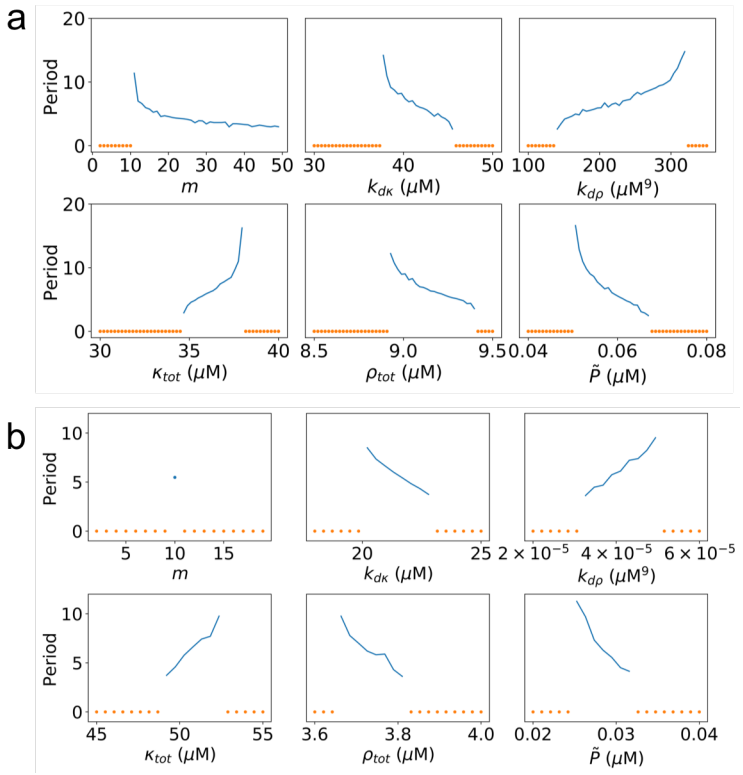

Figure S4: **Robustness analysis for bounded self-assembly system in the limit of fast self-assembly.** In panel **a** we perform robustness analysis as in Figs. S2 and S3 using the first parameter set found yielding oscillations (top row of Table S1). We find that after a threshold at $m = 11$, larger values of m do not appear to preclude oscillations, and oscillation period appears to plateau for large values of m. Oscillations appear most robust to variations in $k_{d\rho}$, which can vary by a factor of ~ 2 in the oscillatory regime. In contrast, all other parameters can vary only by a fraction of their value while maintaining oscillations. In panel **b** we verify similar features in the robustness plot of another randomly and arbitrarily chosen parameter set (the first oscillation found in the second 10^6 parameters screened; sixth row of Table S1); the one significant difference found was that in that parameter set, only $m = 10$ yielded oscillations. These results should be compared to Fig. S2 which show that in the separation-of-timescales limit explored in the main text, oscillations are far more robust: all non-concentration parameters can vary by over an order of magnitude in the oscillatory regime. The relative fragility of oscillations shown in this figure also helps explain the relative paucity of oscillations found using random sampling.

S5 Numerical search for oscillations

In order to determine if a parameter set leads to oscillations, we numerically integrated the differential equations. For bounded self-assembly, we used initial conditions of $(K, P) = (0, 0)$, and for unbounded, $(k, p) = (2\frac{\kappa_{\text{tot}}}{k_{d\kappa}}, 2\frac{\rho_{\text{tot}}}{k_{d\rho}})$. We integrated up to a time determined by the inverse of the minimum timescale in the system. For bounded self-assembly, we integrated up to a time $t_{\text{max}} = 10^3/\min\left(k_{u\kappa}, k_{u\rho}, k_{b\kappa}\kappa_{\text{tot}}^{n-1}, k_{b\rho}\rho_{\text{tot}}^{m-1}\right)$, while for unbounded, we used $t_{\text{max}} = 10^7/\min\left(\eta_{K\kappa}\kappa_{\text{tot}}, \eta_{K\rho}\kappa_{\text{tot}}, \eta_{P\kappa}\rho_{\text{tot}}, \eta_{P\rho}\rho_{\text{tot}}\right)$. For the full system of equations for bounded self-assembly, we used initial conditions corresponding to fully unphosphorylated and unbound κ, ρ, and $\tilde{P}$, and integrated up to

$$t_{\text{max}} = 10^4/\min\left(k_{u\kappa}, k_{u\rho}, k_{b\kappa}\kappa_{\text{tot}}^{n-1}, k_{b\rho}\rho_{\text{tot}}^{m-1}, k_{cK\kappa}, k_{cP\kappa}, k_{cK\rho}, k_{cP\rho}, k_{bK\kappa}\kappa_{\text{tot}}, k_{bP\kappa}\tilde{P}_{\text{tot}}\right).$$

We set the enzyme dissociation constants $k_{uK\kappa}$, $k_{uP\kappa}$, $k_{uK\rho}$, $k_{uP\kappa}$ equal to their respective catalytic rate constants, since the former are largely unspecified by constraints on binding rates and Michaelis constants. Our results are largely insensitive to this assumption. In all cases, the prefactors for t_{max} were determined by applying an order of magnitude larger prefactor and finding no new oscillating solutions.

To determine if the results of the numerical integration can be labeled as oscillations, we used a set of heuristics. We verified these heuristics by plotting solutions found by them to produce oscillations and finding no evidence of false positives. These heuristics considered the behavior of a single system component (e.g. K for bounded self-assembly). First, we determined whether the number of inflection points in the solution is greater than 10. Second, to weed out decaying oscillations, whether the smallest amount by which the component changed between inflection points and the amount it changed between an arbitrarily chosen set of inflection points (between the fifth and sixth) is within $2\times$. Also to weed out decaying oscillations, we measured the amount the component changed between a set of inflection points around the

$3t_{\text{max}}/4$ mark–let's call this amount $x_{3/4}$–and between the penultimate and final inflection point, x_1. We verified that $|(x_{3/4} - x_1)/x_1| < 1$, meaning that the relative change in oscillating height was no more than 100%. We also considered whether the solver required sampling points at a significant frequency (to weed out numerical oscillations): we used the criterion that the third-to-last sampled time point was within 5% of the second-to-last sampled time point. To further root out spurious numerical oscillations we measured the period of the oscillation in two ways–as the time between the third-to-last and last inflection point, and as between the fifth-to-last and third-to-last–and verified that they differed by no more than 1% (parameter sets that fail the equal-period test were integrated for $10\times$ longer and re-tested). Finally, we examined the numerical solution by eye for all parameter sets found to produce oscillations, in order to verify that even if our heuristics produce false negatives (of which we have found almost no evidence) our results contain no false positives.

S6 Supplementary figures

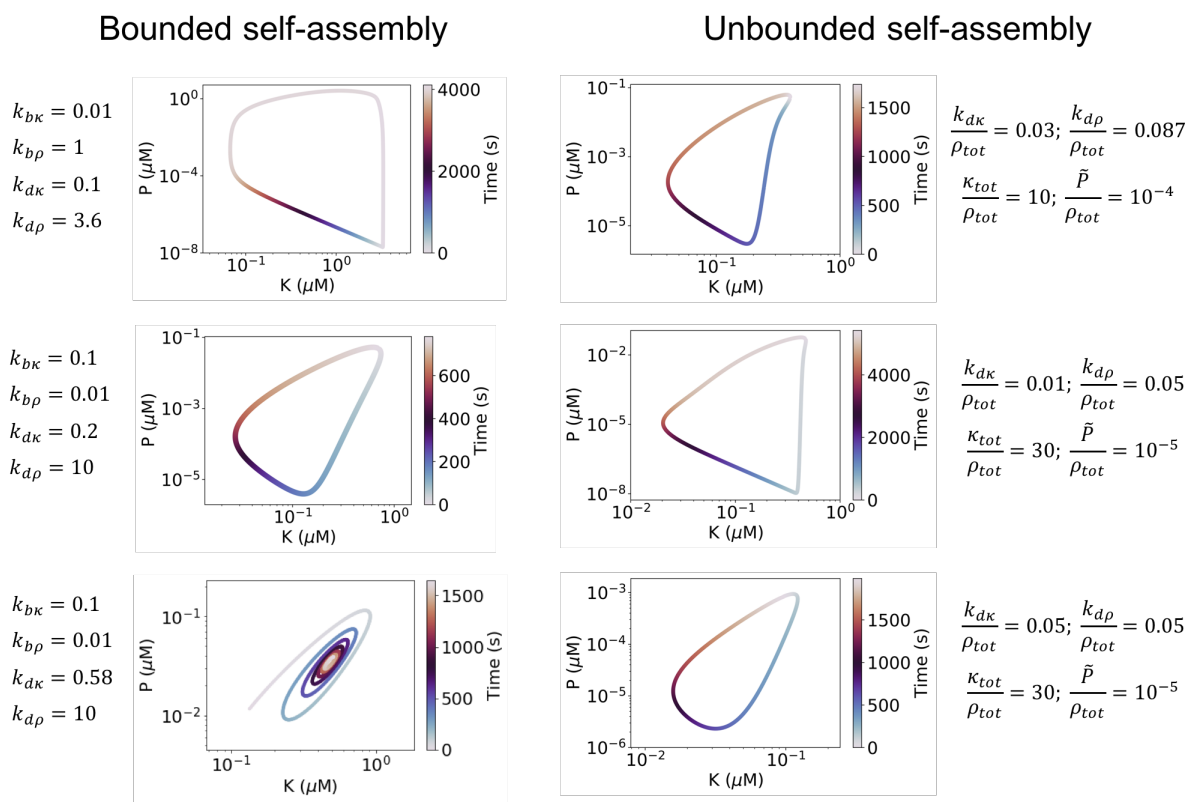

Figure S5: **Example trajectories**. Trajectories displayed in Figs. 2 and 4b are shown along with the parameters used for each trajectory. For trajectories showing sustained oscillations (all but the lower left, which shows a decaying oscillation, and therefore not a desired trajectory) one oscillation cycle is shown.

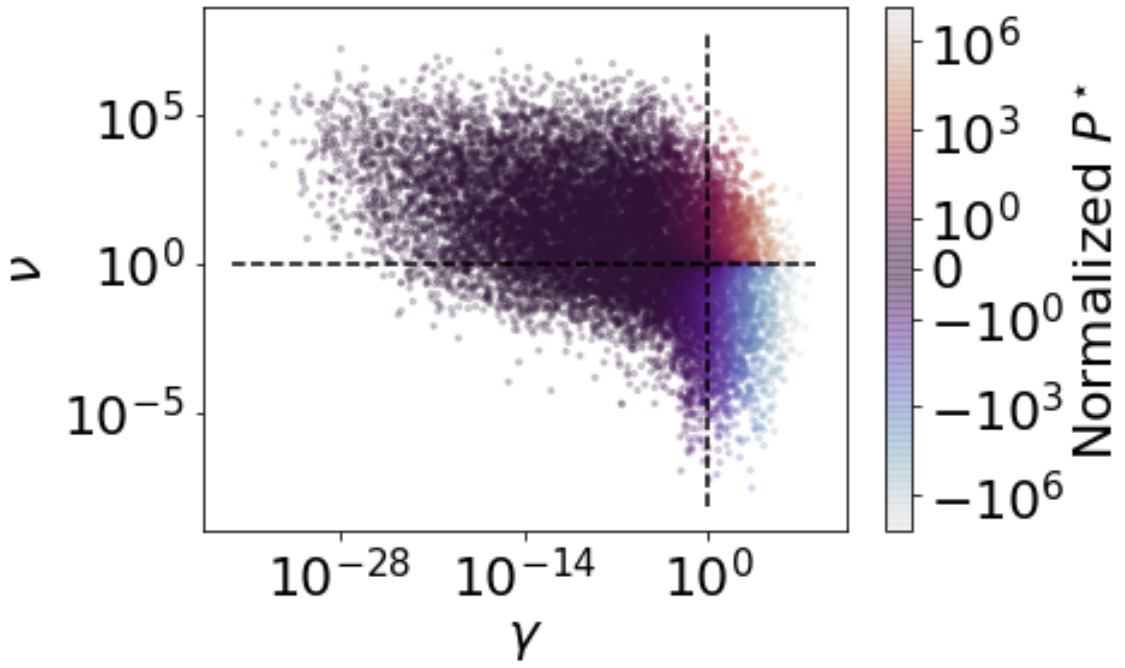

Figure S6: **Verifying Eqn. 4**. Here we plot the parameter sets shown in Fig. 3b in the same phase diagram as that figure, but colorcoded by the normalized steady-state concentration of phosphatase multimer, found using Python's scipy.optimize.root function. In particular, color-coding is given by the left-hand-side of Eqn. 4. Thus, for each parameter set, we show the fixed point concentration of the phosphatase multimer, normalized by the constitutive phosphatase concentration and by a function of the unbinding rates of kinase and phosphatase multimers. The results of this figure demonstrate the validity of our analytical analysis. For large values of γ, the absolute value of normalized $P^\star$ is large; meanwhile, the sign of the normalized $P^\star$ is positive for $\nu > 1$ and negative otherwise. Since oscillations require the normalized value of $P^\star$ to be greater than unity, oscillations are restricted to the upper right quadrant of the phase diagram.

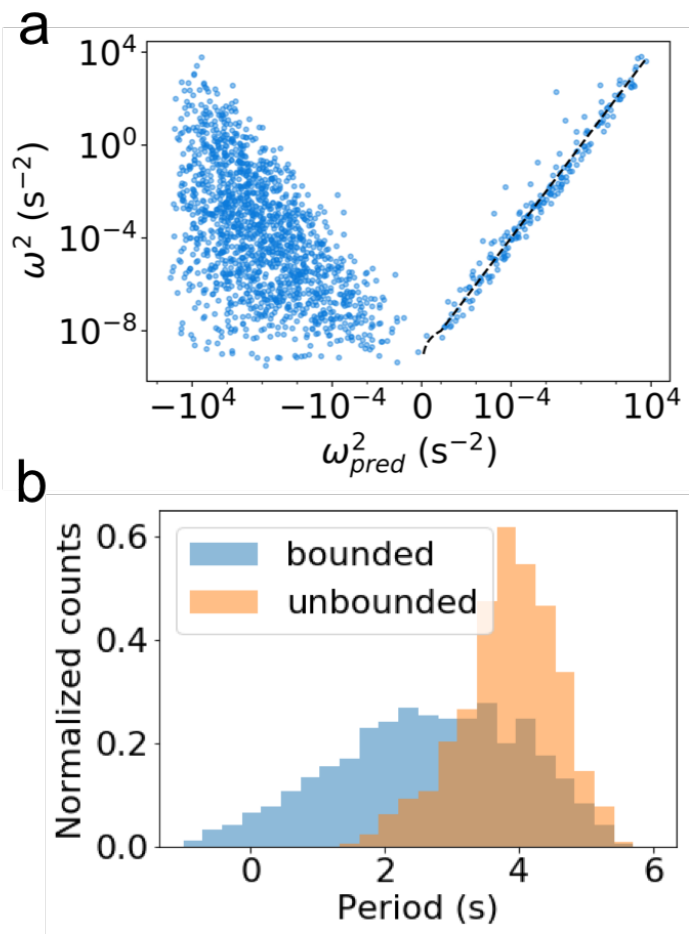

Figure S7: **Oscillation periods. a:** Numerical integration of Eqn. 1 demonstrates Eqn. 6 correctly predicts the frequency of oscillations for the bounded self-assembly system in the linear regime around the fixed point, but is not predictive outside this regime. We make no constraints on the fixed points of the parameter sets considered here. The x-axis shows the predicted squared frequency while the y-axis shows the true squared frequency. For $\omega^2_{\text{pred}} > 0$, the two formulae agree (black dashed line represents $\omega^2 = \omega^2_{\text{pred}}$). For $\omega^2_{\text{pred}} < 0$, ω^2_{pred} is no longer predictive since the oscillations cannot be understood through linear stability analysis of the fixed point. **b:** Random parameters logarithmically distributed within the experimental regime were sampled for Eqns. 1 (bounded self-assembly; blue) and 9 (unbounded self-assembly; orange). The periods of resulting oscillations are histogrammed logarithmically, showing a possible range of periods spanning orders of magnitude, from fractions of a second (minute) for bounded (unbounded) self-assembly, to $>$ 1 day.

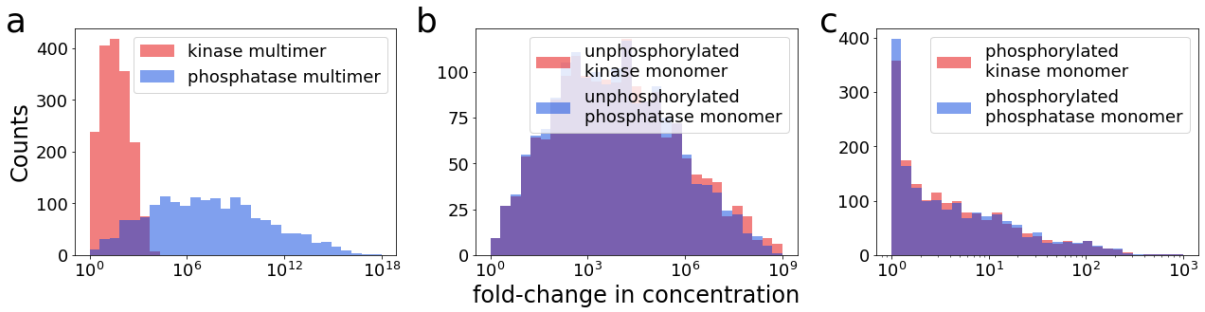

Figure S8: **Amplitude analysis for bounded self-assembly system.** Various experimental tools can be used to visualize the system oscillations. As just two examples, a fluorophore-quencher pair on complementary monomers can enable the visualization of oscillations in monomer concentration, while split fluorophores can enable the visualization of multimer concentrations. Here we numerically integrate oscillating parameter sets found for Eqn. 1, and histogram the amplitude of oscillations of various system components. We define the amplitude here as the maximum concentration divided by the minimum concentration across an oscillatory cycle. We perform this analysis for kinase and phosphatase multimers, unphosphorylated monomers, and phosphorylated monomers. Our results show that typical oscillations involve variation of many orders of magnitude in the concentrations of phosphatase multimers, as well as unphosphorylated kinase and phosphatase monomers. However, these results suggest oscillations cannot be readily visualized using only the concentrations of phosphorylated monomers.

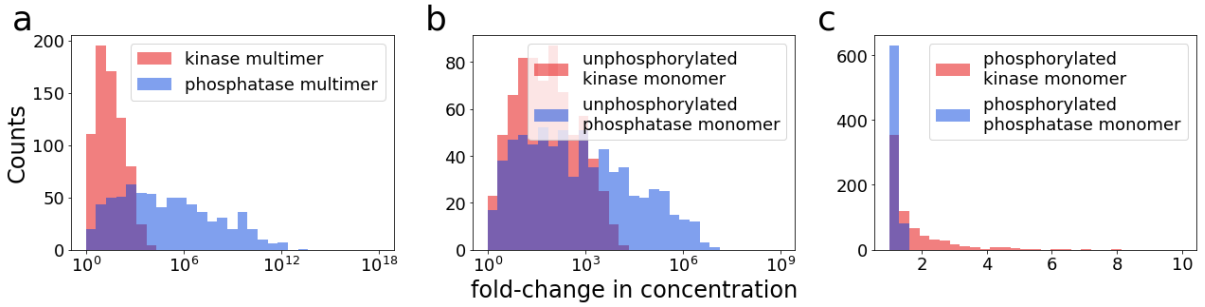

Figure S9: **Amplitude analysis for unbounded self-assembly system.** Analysis performed as in Fig. S8. Our results suggest that oscillations in the concentrations of phosphatase multimers and unphosphorylated monomers should be most readily visible, as they typically vary by several orders of magnitude over an oscillation cycle. Concentrations of kinase multimers and unphosphorylated monomers also typically vary by at least an order of magnitude over an oscillation cycle. Concentrations of phosphorylated monomers typically do not vary by much.

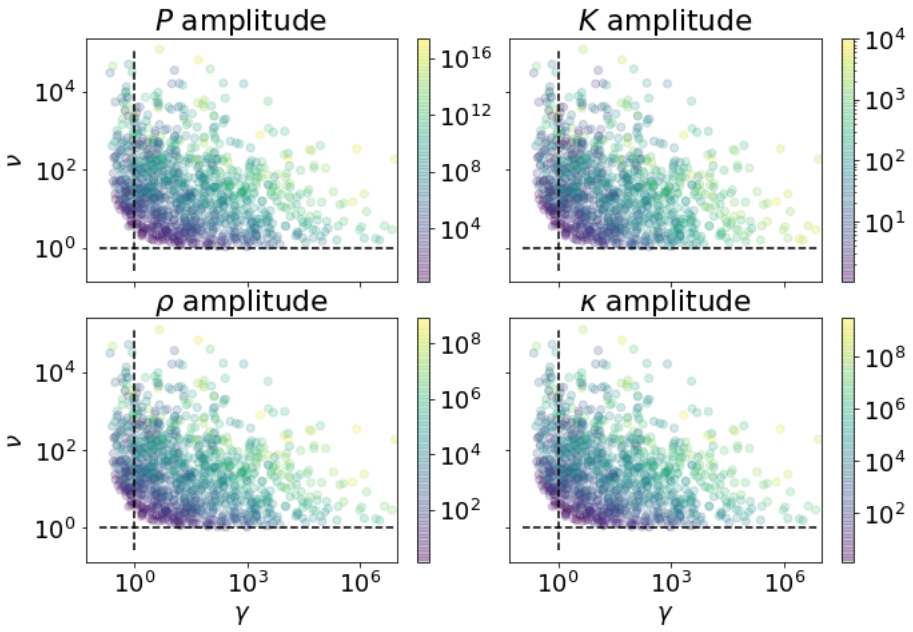

Figure S10: **Amplitudes of bounded self-assembly system oscillations are larger farther from the bifurcation threshold.** Analysis performed as in Fig. S8. Here we show the oscillating parameter sets in γ-ν space, colorcoded by the fold-change in concentration of P, K, ρ, or κ over an oscillatory cycle. Our results demonstrate that parameter sets farther from either bifurcation point ($\gamma = 1$ or $\nu = 1$) typically result in higher amplitudes of oscillations.

REFERENCES AND NOTES

1. O. Purcell, N. J. Savery, C. S. Grierson, M. di Bernardo, A comparative analysis of synthetic genetic oscillators. *J. R. Soc. Int.* **7**, 1503–1524 (2010).

2. M. W. Young, S. A. Kay, Time zones: A comparative genetics of circadian clocks. *Nat. Rev. Genet.* **2**, 702–715 (2001).

3. D. Bray, Protein molecules as computational elements in living cells. *Nature* **376**, 307–312 (1995).

4. X. J. Gao, L. S. Chong, M. S. Kim, M. B. Elowitz, Programmable protein circuits in living cells. *Science* **1258**, 1252–1258 (2018).

5. T. Fink, J. Lonzarić, A. Praznik, T. Plaper, E. Merljak, K. Leben, N. Jerala, T. Lebar, Ž. Strmšek, F. Lapenta, M. Benčina, R. Jerala, Design of fast proteolysis-based signaling and logic circuits in mammalian cells. *Nat. Chem. Biol.* **15**, 115–122 (2018).

6. B. Novák, J. J. Tyson, Design principles of biochemical oscillators. *Nat. Rev. Mol. Cell Biol.* **9**, 981–991 (2008).

7. C. C. Jolley, K. L. Ode, H. R. Ueda, A design principle for a posttranslational biochemical oscillator. *Cell Rep.* **2**, 938–950 (2012).

8. M. Nakajima, K. Imai, H. Ito, T. Nishiwaki, Y. Murayama, H. Iwasaki, T. Oyama, T. Kondo, Reconstitution of circadian oscillation of cyanobacterial KaiC phosphorylation in vitro. *Science* **308**, 414–415 (2005).

9. J. Michael, J. S. Markson, W. S. Lane, D. S. Fisher, E. K. O'Shea, Ordered phosphorylation governs oscillation of a three-protein circadian clock. *Science* **318**, 809–812 (2007).

10. M. J. Rust, Orderly wheels of the cyanobacterial clock. *Proc. Natl. Acad. Sci. U.S.A.* **109**, 16760–16761 (2012).

11. H. Kageyama, T. Nishiwaki, M. Nakajima, H. Iwasaki, T. Oyama, T. Kondo, Cyanobacterial circadian pacemaker: Kai protein complex dynamics in the KaiC phosphorylation cycle in vitro. *Mol. Cell* **23**, 161–171 (2006).

12. S. E. Boyken, M. A. Benhaim, F. Busch, M. Jia, M. J. Bick, H. Choi, J. C. Klima, Z. Chen, C. Walkey, A. Mileant, A. Sahasrabuddhe, K. Y. Wei, E. A. Hodge, S. Byron, A. Quijano-Rubio, B. Sankaran, N. P. King, J. Lippincott-Schwartz, V. H. Wysocki, K. K. Lee, D. Baker, De novo design of tunable, pH-driven conformational changes. *Science* **364**, 658–664 (2019).

13. B. Kholodenko, Negative feedback and ultrasensitivity can bring about oscillations in the mitogen-activated protein kinase cascades. *Eur. J. Biochem.* **267**, 1583–1588 (2000).

14. M. Strumillo, P. Beltrao, Towards the computational design of protein posttranslational regulation. *Bioorg. Med. Chem.* **23**, 2877–2882 (2015).

15. L. Doyle, J. Hallinan, J. Bolduc, F. Parmeggiani, D. Baker, B. L. Stoddard, P. Bradley, Rational design of α-helical tandem repeat proteins with closed architectures. *Nature* **528**, 585–588 (2015).

16. H. Nishi, K. Hashimoto, A. R. Panchenko, Phosphorylation in protein-protein binding: Effect on stability and function. *Structure* **19**, 1807–1815 (2011).

17. H. Nishi, A. Shaytan, A. R. Panchenko, Physicochemical mechanisms of protein regulation by phosphorylation. *Front. Genet.* **5**, 270 (2014).

18. K. Camacho-Soto, J. Castillo-Montoya, B. Tye, I. Ghosh, Ligand-gated split-kinases. *J. Am. Chem. Soc.* **136**, 3995–4002 (2014).

19. K. Camacho-Soto, J. Castillo-Montoya, B. Tye, L. O. Ogunleye, I. Ghosh, Small molecule gated split-tyrosine phosphatases and orthogonal split-tyrosine kinases. *J. Am. Chem. Soc.* **136**, 17078–17086 (2014).

20. Z. Li, S. Liu, Q. Yang, Incoherent inputs enhance the robustness of biological oscillators. *Cell Syst.* **5**, 72–81.e4 (2017).

21. P. Smolen, Frequency selectivity, multistability, and oscillations emerge from models of genetic regulatory systems. *Am. J. Physiol.* **274**, C531–C542 (1998).

22. J. Hasty, M. Dolnik, V. Rottschäfer, J. J. Collins, Synthetic gene network for entraining and amplifying cellular oscillations. *Phys. Rev. Lett.* **88**, 148101 (2002).

23. J. Stricker, S. Cookson, M. R. Bennett, W. H. Mather, L. S. Tsimring, J. Hasty, A fast, robust and tunable synthetic gene oscillator. *Nature* **456**, 516–519 (2008).

24. M. Schlosshauer, D. Baker, Realistic protein-protein association rates from a simple diffusional model neglecting long-range interactions, free energy barriers, and landscape ruggedness. *Protein Sci.* **13**, 1660–1669 (2004).

25. S. E. A. Ozbabacan, H. B. Engin, A. Gursoy, O. Keskin, Transient protein–protein interactions. *Protein Eng. Des. Sel.* **24**, 635–648 (2011).

26. S. Zhuo, J. C. Clemens, R. L. Stone, J. E. Dixon, Mutational analysis of a Ser/Thr phosphatase. *J. Biol. Chem.* **269**, 26234–26238 (1994).

27. C. Chen, B. H. Ha, A. F. Thévenin, H. J. Lou, R. Zhang, K. Y. Yip, J. R. Peterson, M. Gerstein, P. M. Kim, P. Filippakopoulos, S. Knapp, T. J. Boggon, B. E. Turk, Identification of a major determinant for serine-threonine kinase phosphoacceptor specificity. *Mol. Cell* **53**, 140–147 (2014).

28. R. A. Langan, S. E. Boyken, A. H. Ng, J. A. Samson, G. Dods, A. M. Westbrook, T. H. Nguyen, M. J. Lajoie, Z. Chen, S. Berger, V. K. Mulligan, J. E. Dueber, W. R. P. Novak, H. El-Samad, D. Baker, De novo design of bioactive protein switches. *Nature* **572**, 205–210 (2019).

29. A. H. Ng, T. H. Nguyen, M. Gómez-Schiavon, G. Dods, R. A. Langan, S. E. Boyken, J. A. Samson, L. M. Waldburger, J. E. Dueber, D. Baker, H. El-Samad, Modular and tunable biological feedback control using a de novo protein switch. *Nature* **572**, 265–269 (2019).